POLITECNICO DI TORINO

Master Degree Environmental and Land Engineering - Climate Change

Master Degree Thesis

Soil water balance in rice fields: modelling and irrigation management in a Piedmont area

Supervisors
Stefania Tamea
Amirarsalan Shahmohammadi

Candidate
Graziano Miccolis

Academic Year 2024-2025

Abstract

Variations in rainfall and temperature due to climate change, combined with unsustainable water consumption patterns, are affecting water availability. According to the Global Environmental Outlook 2000 of the United Nations Environment Programme (UNEP), water scarcity can be considered as one of the most critical environmental issues of the 21st century and will negatively impact all sectors. Water scarcity and increasing competition for water resources pose critical challenges to agriculture, particularly for water-intensive crops such as rice. In this context, assessing irrigation requirements is essential for the development of effective water-related policies and for optimizing irrigation management, ensuring sustainable water use and preserving agricultural productivity. This thesis develops a Python-based soil water balance model specifically designed for paddy rice, extending an existing high-resolution framework for the assessment of irrigation requirements and adapting it to the conditions of the Piedmont area. In particular the pilot area where the model was applied is the Associazione d'Irrigazione Ovest Sesia (AIOS) district in Piemonte, a 100,000-hectare area where rice covers about 75% of the cultivated land. The model performs a daily soil water balance coupled to vegetation dynamics by integrating climatic, soil, and crop parameters to simulate soil moisture and saturated water level dynamics throughout the growing season based on FAO guidelines. Input data include: i) downscaled ERA5-based climatic data (2.2 km), ii) Soil physical and hydraulic properties from SoilGrids and HIhydrodata, iii) regional Agricultural Land Use data from the Geoportale Piemonte (cadastral mosaic, SigmaTer project) and iv) local crop and irrigation information from district technicians and previous studies in nearby areas. The irrigation requirements obtained from the model, organized on a spatial grids covering the main rice-cropped area in North Italy, are coupled with GIS analysis to compute irrigation depths and volumes at the district scale. Three irrigation strategies were simulated—Continuous Flooding (CF), Alternate Wetting and Drying (AWD), and Dry Seeding with Delayed Flooding (DFL). Despite some limitations introduced in the water balance and in relation to groundwater, the model produced results consistent with previous studies. Both Alternate wetting-drying and Dry Seeding strategies reduce the district irrigation requirements compared to Continuous Flooding, with the second providing the largest overall water savings. However, Dry seeding increases water demand during critical summer months (June–July) and limits early-season groundwater recharge, which may otherwise support the soil water balance in downstream areas. These findings highlight the model's reliability and potential for scenario analyses aimed at improving sustainable water management in rice-growing regions.

Contents

Chapter 1

Introduction

Water has always been considered the fundamental resource without which life on Earth would not be possible. Throughout history, the development of human societies has been closely linked to the management and availability of this essential resource. Today more than ever, this resource is under threat. Human activities are altering the Earth's climate system and the water cycle, and when combined with the unsustainable use of water, this has led to a real water crisis [1]. Currently, more than four billion people — around two-thirds of the global population — experience severe water scarcity. In 2018, 2.3 billion people were living in countries under water stress, and 3.6 billion had inadequate access to water for at least one month per year. By 2050, this number is expected to exceed five billion, due to population growth and the resulting increase in water demand [2]. According to the Global Environmental Outlook 2000 of the United Nations Environment Programme (UNEP), freshwater scarcity is considered by scientists and policymakers to be the second most critical environmental issue of the 21st century just after Global Warming [3]. Water scarcity has a significant impact on various socio-economic sectors, especially those with the highest water consumption. At the same time, water reserves are also heavily affected by these same sectors. Among the sectors most affected by — and simultaneously most responsible for — water use is agriculture. According to FAO data, agriculture accounts for approximately 70% of global freshwater withdrawals on average, mainly due to irrigation practices. Over the past thirty years, food production has more than doubled, and FAO estimates that around 60% more food will be needed by 2050 to meet the needs of a growing global population. As a result, the necessity to increase food production — combined with the effects of climate change— means that water demand is expected to rise significantly [4]. Among all the different type of crops, rice is the one that can be considered the most critical than others in terms of irrigation requirements. It is considered the main food source consumed by more than half of the global population. At the same time it accounts for the majority of the agricultural irrigation water requirements, beeing a flooded cultivation[5]. In fact in traditional irrigation management strategy, the field remains under water for almost the whole season. For this reason, even if rice has a similar physiological water productivity to other main cereals, its cultivation demands much larger amounts of water, making rice paddies responsible for about 40% of the world's total irrigation water use[6]. Global

warming, combined with the increasing competition for water between lowland rice and other seasonal crops, as well as industrial and urban demands, may lead to both physical and economic water scarcity for rice cultivation[7]. Projections indicate that by 2050, many of the lowland irrigated rice regions currently in use will suffer from significant water shortages [8].

While Asia remains the leading rice producer, rice also represents an important economic asset in Europe, particularly in the Mediterranean region. The Mediterranean basin hosts approximately 1.3 million hectares of rice fields, with Italy representing the core of European production. Accounting for more than half of the EU's total rice output, Italy combines both high productivity and quality standards, ranking second only to Egypt within the Mediterranean region. Most of the national rice cultivation is concentrated in the Po Valley, particularly along the left bank of the Po and the Ticino rivers, across Lombardy and Piedmont. In 2017, this area covered about 213,000 hectares, corresponding to roughly 93% of Italy's total rice-growing surface[9]. Consequently, for these regions, the development of solutions and strategies aimed at ensuring the long-term sustainability of rice cultivation and preventing potential water-related issues is of crucial importance. In recent years, these needs have led to the adoption and investigation of alternative irrigation methods to the traditional continuous flooding system. Among the most significant practices are: i) DLF (Delayed Late Flooding), which involves dry seeding followed by a delayed flooding stage; and ii) AWD (Alternate Wetting and Drying), which consists of wet seeding combined with alternating cycles of soil drying and re-flooding. In this context, the study of the irrigation requirements becomes essential to optimize agricultural productivity especially for paddy rices. Assessing irrigation requirements is crucial for managing water more efficiently, avoiding waste, reducing consumption, and maintaining high productivity levels [10]. Studies shown that the volume of water withdrawn for agriculture could be limited to only a 10% increase, to satisfy the increase by 60% by 2050 in food demand, provided that more efficient irrigation practices are implemented and crop yields are improved [4]. Information on present and historical water use is often scarce or incomplete and modelling current irrigation water needs provides the foundation for estimating the future impact of climate change, as well as demographic, socioeconomic, and technological shifts.

This Thesis addresses the challenging context outlined above. It builds upon the high-resolution water-balance framework proposed by Rolle et al. [10], extending and adapting it to develop a dedicated model for paddy rice. A Python-based soil water balance model - coupled with vegetation dynamics - for rice is therefore developed. The model is then applied on an high density rice cultivated area in Piemonte region, providing spatially explicit assessments of rice water requirements to support scenario analysis and operational planning at the district level. Different irrigation strategies (CF, AWD, DLF) have been evaluated in order to assess their influence on irrigation volumes and the potential for reducing water consumption without compromising crop performance.

Chapter 2

Background

2.1 Water requirements and Evapotranspiration

In general, irrigation requirement is defined as the additional amount of water that must be supplied to crops when precipitation alone is insufficient to meet their evapotranspiration demand[10]. Consequently, in order to determine the amount of water that must be supplied through irrigation to compensate for losses and ensure healthy and optimal crop growth, it is necessary to calculate the water evapotranspired by the plant.

Evapotranspiration (ET) represents the combined processes of *evaporation* and *transpiration*, through which water changes from liquid to vapour and is transferred to the atmosphere.

Evaporation refers to the vaporization of liquid water from exposed surfaces such as soil, water bodies, or wet vegetation. This process requires energy mainly supplied by solar radiation and, to a lesser extent, by air temperature. The rate of evaporation depends on the vapour pressure gradient between the evaporating surface and the surrounding air, and it is strongly influenced by climatic variables such as solar radiation, air temperature, humidity, and wind speed. When the soil surface is wet, evaporation is governed mainly by meteorological conditions, whereas under dry conditions it becomes limited by soil water availability.

Transpiration instead is the vaporization of water contained within plant tissues that is transpired through stomata, which consist in small openings on the leaves that regulate gas and vapour exchange. Water absorbed by the roots moves through the plant and is released as vapour into the atmosphere. The rate of transpiration depends not only on climatic factors (radiation, humidity, temperature, and wind) but also on soil moisture, crop type, growth stage, and management practices.

Evaporation and transpiration occur simultaneously and are difficult to distinguish in practice. At the beginning of the crop cycle, when vegetation cover is limited, most evapotranspiration originates from soil evaporation. As the crop develops and the leaf area index (LAI) increases, transpiration becomes the dominant process. As illustrated in Figure 2.1, at sowing nearly all ET results from evaporation, whereas during full canopy cover more than 90% of ET derives from transpiration[11].

In this context, a major contribution has been provided by the FAO Irrigation and

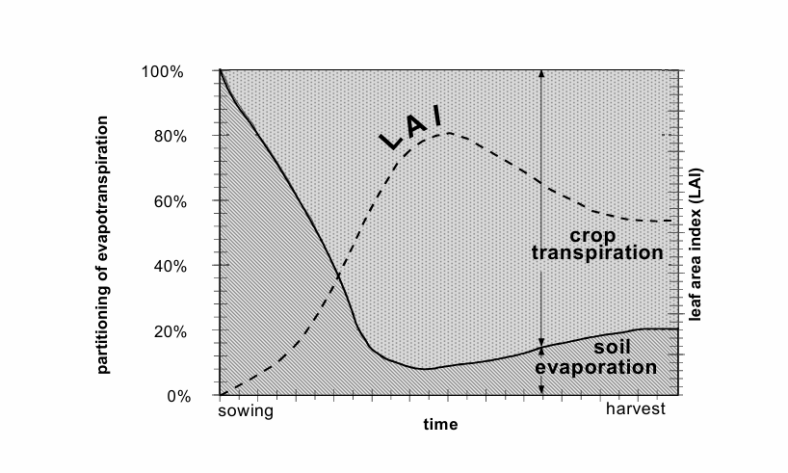

Figure 2.1: The partitioning of evapotranspiration into evaporation and transpiration over the growing period for an annual field crop [11]

.

Drainage Paper No. 56 [11]. FAO-56 has become the international guideline for the development of water balance models aimed at estimating irrigation requirements. The document establishes the procedure for calculating actual evapotranspiration (ETa) starting from a reference evapotranspiration value multiplied by two coefficients, Kc and Ks. The reference evapotranspiration is defined as the evapotranspiration rate [mm/day] from a hypothetical well-watered grass surface with fixed characteristics.

The concept was developed to represent the atmospheric evaporative demand independently of crop type, growth stage, or management practices as well as providing the basis for estimating crop-specific water use. Several approaches have been proposed for estimating ET0; The FAO Penman–Monteith (PM) equation is recommended as the standard method. This method was chosen because it provides a close approximation of grass reference ET0 under diverse conditions, is physically consistent, and explicitly accounts for both physiological and aerodynamic factors. Its computation through the FAO Penman–Monteith method requires meteorological inputs such as air temperature, relative humidity, solar radiation, and wind speed, which can be processed at various time scales (daily, weekly, ten-day, or monthly). To ensure reliable results, these measurements should be taken or adjusted to a reference height of 2 m above a surface of well-watered grass[11]. The FAO Penman-Monteith equation to estimate ETo is:

$$ET_0 = \frac{0.408\,\Delta(R_n - G) + \gamma\,\frac{900}{T+273}\,u_2\,(e_s - e_a)}{\Delta + \gamma\,(1 + 0.34\,u_2)} \tag{2.1}$$

where:

- ET_0 = reference evapotranspiration [mm day^{-1}]
- R_n = net radiation at the crop surface [MJ m^{-2} day^{-1}]
- G = soil heat flux density [MJ m^{-2} day^{-1}]

- T = mean daily air temperature at 2 m height [°C]
- u_2 = wind speed at 2 m height [m s^{-1}]
- e_s = saturation vapour pressure [kPa]
- e_a = actual vapour pressure [kPa]
- $e_s - e_a$ = saturation vapour pressure deficit [kPa]
- Δ = slope of vapour pressure curve [kPa $°C^{-1}$]
- γ = psychrometric constant [kPa $°C^{-1}$]

Although the FAO Penman–Monteith equation is the recommended standard for estimating reference evapotranspiration, alternative approaches have also been proposed, as highlighted in the previous table. One widely used example is the Hargreaves method, introduced by Hargreaves and Samani. This is a temperature-based empirical model in which reference evapotranspiration (ETo) is related to solar radiation and mean air temperature. The formulation was originally derived from regression analysis of eight years of lysimeter measurements for a grass reference crop in Davis, California, and was later validated in different climatic contexts worldwide[12].

The Hargreaves equation expresses ETo as:

$$ET_0 = K \cdot R_s \cdot (T + 17.8) \tag{2.2}$$

where K is an empirical coefficient, Rs is solar radiation, and T is the mean daily air temperature. Because radiation data are not always available, Hargreaves and Samani also proposed an auxiliary equation to estimate solar radiation (Rs) from extraterrestrial radiation (Ra) and the difference between daily maximum and minimum temperature[12]:

$$R_s = K_{RS} \cdot R_a \cdot \sqrt{T_{max} - T_{min}} \tag{2.3}$$

where Krs is a calibration coefficient, and Tmax and Tmin are the daily maximum and minimum air temperatures.

By combining the two equations, ET0 can be calculated by the compact formulation presented by Hargreaves and Allen (2003)[12]:

$$ET_0 = K_{RS} \cdot K \cdot R_a \cdot (T + 17.8) \cdot \sqrt{T_{max} - T_{min}} \tag{2.4}$$

This method is particularly useful in data-scarce regions, since it requires only temperature observations, while still capturing short-term variability in evapotranspiration and being applicable to sub-daily time steps[12].

Another commonly used approach is the Priestley–Taylor method (Priestley and Taylor, 1972), which represents a simplified form of the surface energy balance for estimating evapotranspiration. The equation was derived from experimental data collected at different sites under saturated soil or open water conditions, in the absence of significant advection. It provides a practical relationship between sensible and latent heat fluxes.

For partially saturated land surfaces, the reference evapotranspiration (ETo) is estimated as a fraction of the equilibrium evapotranspiration, using a proportionality coefficient alpha[12] :

$$ET_0 = \alpha \cdot \frac{(R - G) \cdot \Delta}{\Delta + \gamma} \tag{2.5}$$

where:

- ET_0 = reference evapotranspiration [mm day^{-1}]
- α = Priestley–Taylor coefficient (dryness coefficient), typically around 1.26 under saturated conditions
- R = net incoming radiation [MJ m^{-2} day^{-1}]
- G = soil heat flux into the ground [MJ m^{-2} day^{-1}]
- H = sensible heat flux [MJ m^{-2} day^{-1}]
- LE = latent heat flux [MJ m^{-2} day^{-1}], with $R - G = LE + H$
- Δ = slope of the saturation vapour pressure curve [kPa °C^{-1}]
- γ = psychrometric constant [kPa °C^{-1}]

Another method used to estimate evapotranspiration is the Surface Energy Balance (SEB) approach. The method is based on the principle that the available net radiation at the land surface is partitioned into different fluxes: sensible heat, latent heat (evapotranspiration), and soil heat flux[13]. In its simplest form, the energy balance equation can be expressed as:

$$R_n = H + LE + G \tag{2.6}$$

where:

- R_n = net radiation at the surface [W m^{-2}]
- H = sensible heat flux [W m^{-2}]
- LE = latent heat flux, related to evapotranspiration [W m^{-2}]
- G = soil heat flux [W m^{-2}]

In practice, the latent heat flux (and thus evapotranspiration) is often obtained as the residual term of the energy balance, once R_n, G, and H are estimated.

- R_n and G can be derived from ground or remote sensing data (e.g., radiation, albedo, surface emissivity).

- H is usually calculated using the difference between surface and air temperatures, together with aerodynamic resistance formulations.

Different implementations of the SEB method exist:

- **Single-source models**, which treat the land surface (soil + vegetation) as a single layer.
- **Two-source models**, which separately simulate the exchanges from soil and vegetation, improving accuracy in partially vegetated areas.
- **Advanced versions**, such as SEB-A (Surface Energy Balance with Advection), which explicitly account for horizontal advection by distinguishing between a "local" ET driven by radiation balance and an "exotic" ET due to advected energy.

The SEB method is particularly suited for remote sensing applications, as it can integrate satellite-derived land surface temperature, albedo, and vegetation indices with meteorological observations to provide spatially distributed estimates of evapotranspiration[13].

At this stage, it is possible to move from the reference evapotranspiration (ET0) to a value that accounts for the specific characteristics of a given crop, known as the **crop evapotranspiration (ETc)**.

It is done by integrating the **crop coefficient (Kc)**. It accounts for the specific characteristics of the crop throughout its growth stages and allows the estimation of crop evapotranspiration under optimal soil moisture and, more generally, under standard conditions. With this approach, crop evapotranspiration is calculated as:

$$ET_c = K_c \times ET_o \tag{2.7}$$

This crop-related effect can be represented using a single crop coefficient (K_c) directly influencing the overall Evapotranspiration or separated into two components through the **dual crop coefficient approach**, where:

$$K_c = K_{cb} + K_e \tag{2.8}$$

K_{cb} represents the *basal crop coefficient*, associated with plant transpiration, while K_e is the *soil evaporation coefficient*, which accounts for direct soil evaporation. In this dual approach, the soil profile is conceptually divided into two layers:

- a **subsoil layer**, corresponding to the root zone, where water uptake drives transpiration (K_{cb});
- a **topsoil layer**, typically the upper 10 cm, from which direct evaporation occurs (K_e).

The crop coefficient (K_c) varies throughout the growing season, reflecting the evolution of canopy development and soil moisture conditions. It starts from wide variable values at the beginning of the season, depending on whether the soil surface is dry or wet

(as in flooded crops). This happens since during the early growth stages, evapotranspiration is mainly governed by *soil evaporation*, since the crop is still small, the root system is shallow, and transpiration remains limited. Consequently, the initial K_c values—both in the single and dual coefficient approaches—depend largely on the amount of water available for evaporation at the soil surface.

As the crop develops, with increasing height and green canopy, transpiration gradually becomes the dominant process, reaching its peak during the mid-season stage, when the vegetation fully covers the soil. At this point, soil evaporation becomes minimal as the shaded soil surface limits direct exposure to solar radiation.

In the late-season or ripening stage, K_c typically decreases as the crop approaches maturity and its physiological activity declines, with the extent of this reduction depending on the harvest date and crop type.

Figures 2.3, 2.4 illustrate the typical seasonal trend of the crop coefficient (K_c) and the relative contributions of evaporation and transpiration during the different growth stages, as a function of canopy development and vegetation cover.

Then the water stress coefficient (Ks) can be introduced to consider situations where soil moisture drops below field capacity and can reach the critical threshold, defined as the wilting point. The integration of this additional coefficient makes it possible to estimate the actual evapotranspiration (ETa or ETc adj)[11]. The parameter can range between 1 and 0, where the first value corresponds to no water stress while the second refers to total water stress. Then the actual Evapotranspiration (Eta) can be computed as follow:

$$ET_a = K_c \times K_s \times ET_o \tag{2.9}$$

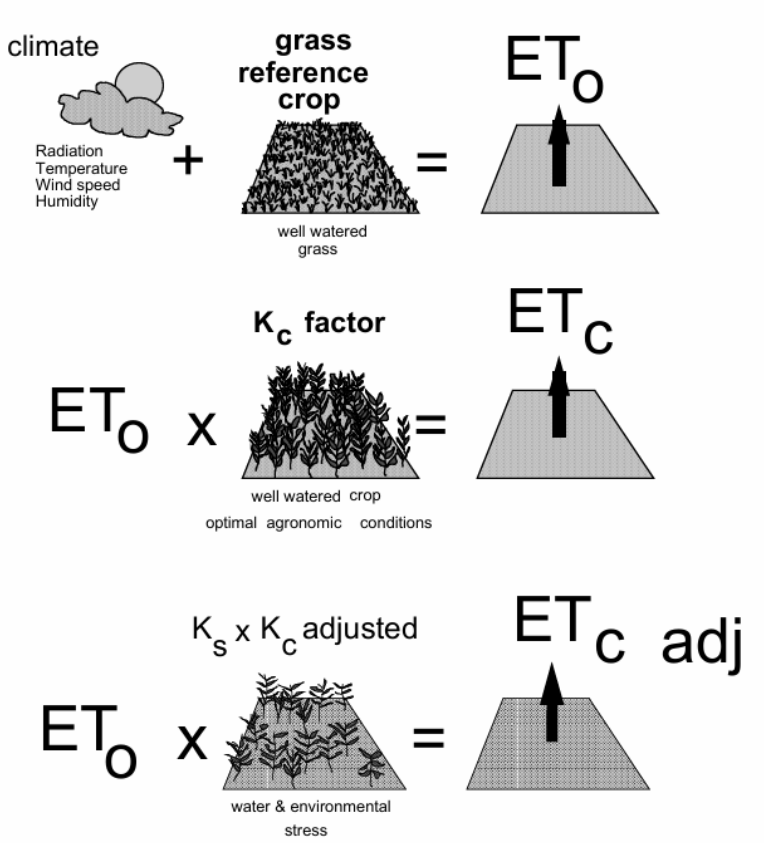

Figure 2.2: Reference (ETo), crop evapotranspiration under standard (ETc) and non-standard conditions (ETc adj)[11].

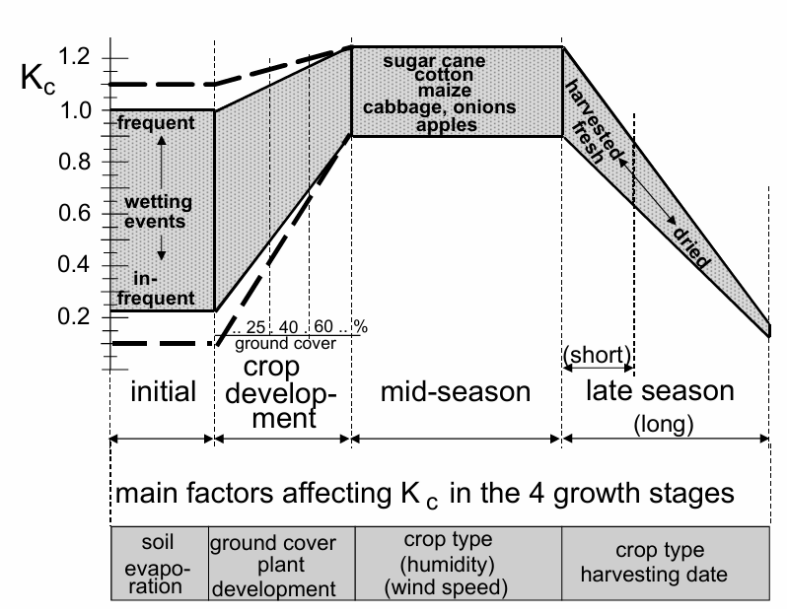

Figure 2.3: Typical ranges expected in Kc for the four growth stages[11].

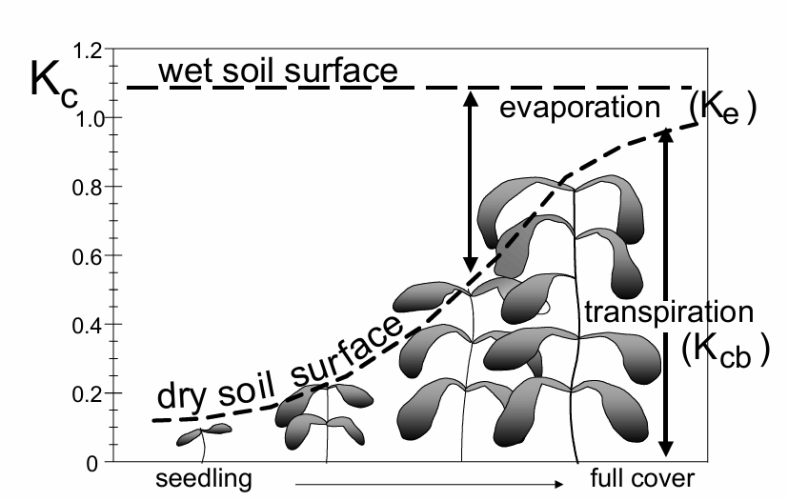

Figure 2.4: The effect of evaporation on the crop coefficient (Kc). The horizontal line represents the Kc value under conditions of a continuously wet soil surface, while the curved line refers to the case where the soil surface remains dry but the crop receives sufficient water to sustain full transpiration[11].

2.2 State of the Art

Over the last decades, the estimation of irrigation water requirements has been the subject of extensive research at both global and regional scales. The main objective of these studies is to quantify the volume of water that must be supplied to crops when precipitation is not sufficient to meet evapotranspiration demand.

The earliest global assessments were based on models such as WaterGAP[14], WATERSIM[15], LPJmL[16], and H07[17], which provided valuable large-scale insights but often did not account for multi-cropping systems, the succession of multiple growing cycles on the same land, and offered limited crop-specific differentiation.

Developments in data availability and modeling methodologies led to more refined global frameworks, including GCWM[18], GEPIC[19], the FAO's CROPWAT[20], and WATNEEDS[21]. These studies typically focused on the year 2000, when detailed spatial information on irrigated areas became globally available. As summarized in the table 2.7, the spatial resolution of global irrigation models has progressively improved thanks to the release of more detailed datasets describing irrigated croplands and climate inputs. However, the majority of these models still rely on relatively coarse spatial grids or on monthly climatic data, which limits their ability to capture short-term hydroclimatic variability and therefore to produce usefull insigths for irrigation management purposes.

In this context, the high-resolution water balance model proposed by Rolle et al.(2021) [10] represents a significant advancement. The model integrates daily global datasets for both precipitation and reference evapotranspiration, computed on a fine-resolution grid to better represent spatial variability in irrigation demand. Reference evapotranspiration is estimated using temperature-based calculations according to the Hargreaves–Samani.

The model applies a soil–water balance approach derived from FAO methodology to estimate irrigation requirements worldwide. Its application focuses on the year 2000, in alignment with the MIRCA2000 dataset, which provides global coverage for 26 major irrigated crops. The resulting irrigation estimates were compared with outputs from other global models as well as with observed irrigation volumes across multiple spatial scales, demonstrating the advantages of employing high-resolution, daily climatic data in global water resource assessments[10].

Global Models		Spatial resolution	Base year	MCP	Precipitation	Reference evapotranspiration	
2021	**This study**	**0.0833°**	**2000**	**yes**	**0.25° (d)**	**0.25° (d)**	**HS**
2020	WATNEEDS	0.0833°	2000[(a)], 2016	yes	0.05° (d), 0.5° (d)*	0.5° (m)	PM
2011	CROPWAT (FAO)	0.0833°	2000[(b)]	no	0.5° (m)	0.166° (m-LTA)	PM
2010	GEPIC	0.5°	2000	yes	0.5° (m)	0.5° (m)	HS
2010	GCWM	0.0833°	2000[(a)]	yes	0.5° (m), 0.166° (m-LTA)**	0.5° (m), 0.166° (m-LTA)**	PT, PM
2008	H07	1°	1991[(c)]	no	1° (d)	1° (d)	SEB
2008	LPJmL	0.5°	1985[(d)]	no	0.5° (m)	0.5° (m)	PM
2007	WATERSIM (IWM)	0.1°	2000	no	0.5° (m)	0.5° (m)	PM
2002	WaterGAP	0.5°	1995	no	0.166° (m-LTA)	0.166° (m-LTA)	PT

Figure 2.5: Summary of models that estimate global irrigation requirement from [10].

2.3 Rice Irrigation strategies

Rice, wheat, and maize represent the most important irrigated crops worldwide, cultivated on approximately 102,000, 75,000, and 31,500 thousand hectares, respectively. Together they account for nearly half of the global dietary energy supply, with rice alone providing more than 20% of global caloric intake and serving as a staple food for over 3.5 billion people, particularly in developing countries. Traditional rice cultivation, however, is highly water demanding, as it relies on maintaining flooded fields from seeding to harvest. Compared to other cereals, this practice requires substantially larger volumes of irrigation water, placing rice among the most water-consuming crops at the global scale[22].

In light of increasing water scarcity and competition for resources, researchers have devoted significant effort to exploring alternative irrigation strategies to continuous flooding (WFL), aiming to enhance water use efficiency while sustaining yields[23].

Among the most efficient and increasingly studied water-saving practices is the Alternate Wetting and Drying (AWD) technique. Under this method, rice paddies are not kept continuously flooded but undergo cycles of wetting and drying, with irrigation applied only when the soil water status reaches a predefined threshold to restore the initial ponding water. This threshold can be expressed in terms of soil water potential or soil water content in the root zone (SWP, SWC), or alternatively as the depth of the perched water table below the soil surface (WLD)[23]. AWD can be initiated a few weeks after sowing. The number of days of non-flooded soil in AWD between irrigations can vary from 1 day to more than 10 days depending on the soil type[24].

In the literature, two main types of AWD are usually distinguished:

- mild or safe AWD, where SWP is kept between soil saturation and -20 KPa (WLD < 15 cm).
- severe AWD, where SWP drops below -20 KPa (WLD $< 20/25$ cm) [23]

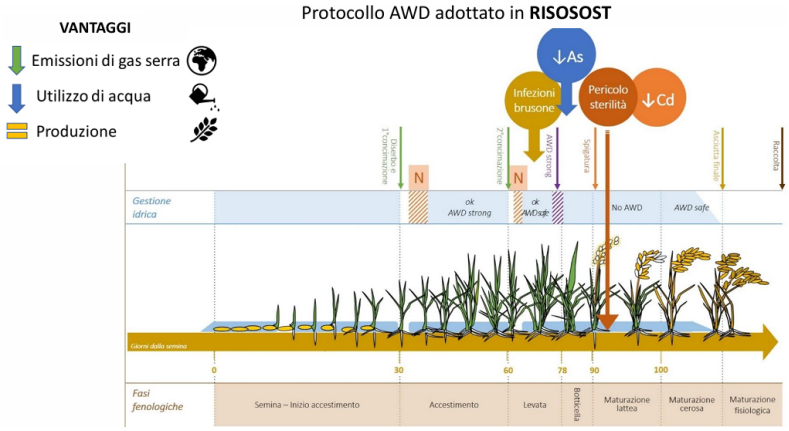

Figure 2.6: AWD (Alternate Wetting and Drying) protocol adopted within the RISOSOST project. The scheme illustrates water management during the different phenological stages of rice. [25]

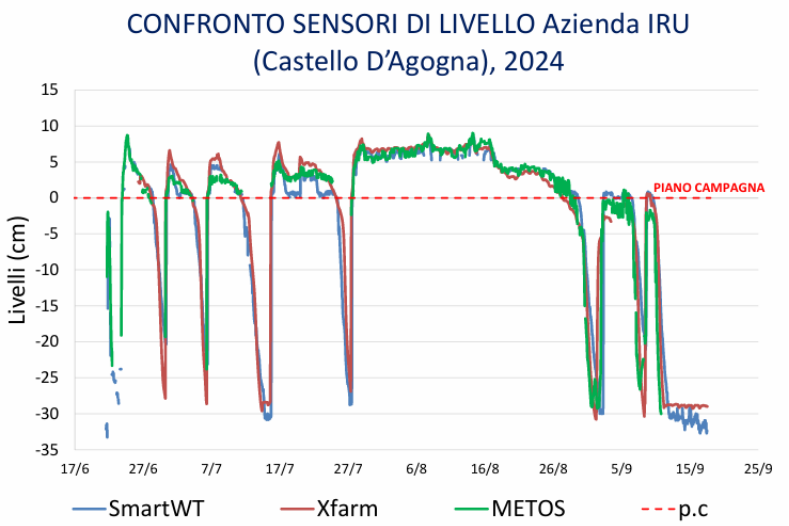

Figure 2.7: Field demonstration of AWD water management at the IRU farm (Castello D'Agogna, 2024). The graph shows water level fluctuations measured by different sensors (SmartWT, Xfarm, METOS), illustrating the typical alternation of flooding and drying cycles occurring under AWD in real conditions. [25]

Numerous field studies have investigated the effects of AWD on both environmental and agronomic aspects, considering its timing within the crop cycle as well as the severity of the thresholds adopted. A comprehensive review of 56 studies, comprising 528 comparisons between AWD and continuous flooding (WFL), highlighted that when AWD is implemented under "safe" conditions, rice yields remain largely unaffected while average water use (irrigation plus rainfall) can be reduced by about 23% [26].

AWD is not the only approach that has been investigated in recent years. Other strategies include dry seeding with delayed flooding (DFL), dry seeding combined with

fixed-turn irrigation (FTI), and early dry seeding with delayed flooding (DFLearly). Several studies shown that these dry-seeding solutions can help to further reduce the rice water demand. This mainly occur since with these options the field is not flooded before seeding, unlike AWD and WFL. The seeding occurs on dry soil. This means that the field is not in saturation and ponding water is not present but the soil can be anyway wetted befor sowing. Then it is flooded about one month after seeding in DFL or it's wetted by fixed-turn irrigation with FTI. On the other hand, these studies [23, 9] have shown that dry-seeding techniques can increase water demand during the most critical months (June–August), when competition with other major crops is highest. Moreover, they reduce the groundwater recharge that typically occurs in spring under wet-seeding conditions, preventing any rise in the groundwater level (GWL). A shallow GWL is generally beneficial for crops—especially in downstream areas—as it helps lower irrigation needs [23].

Innovative techniques like AWD and DFL have also an impact on GHG's emissions from paddy rice. Rice cultivated in continuous flooding conditions produce significant amount of Methane (CH4) emissions. This is mainly due to the anaerobic decomposition of organic matter and crop residues by methanogenic microorganisms. At global level, Methane's emissions represent the main contribution of rice cultivation to Climate Change. It accounts for almost 27 milions of ton of CH4 per year which represents about the 9% of anthropogenic CH4 emissions every years. In Italy rice cultivation generates 54000 ton of methane every years, which represents the 3.4% of national CH4 emissions [27]. The dry seeding and late flooding (DFL) can help to reduce the emissions by about 56% [28]. Alternate Wetting and Drying (AWD) techniques are widely recognized as the most promising practice for reducing greenhouse gas emissions in rice cultivation. They significantly mitigate CH4 emissions compared to continuous flooding, especially when the strictest regime (AWDstrong) is applied. Conversely, the alternation between flooded and dry conditions may lead to a slight increase in cumulative N2O emissions, which nevertheless remain at very low levels. Overall, the adoption of the AWD technique reduces the Global Warming Potential (GWP) by approximately 35–54% compared to continuous flooding [29].

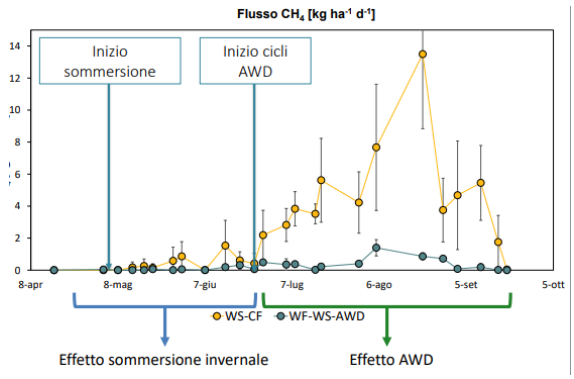

Figure 2.8: CH4 reduction effect of AWD irrigation strategy [29].

The efficiency of each strategy depends on local factors such as soil permeability, topography, and groundwater depth. Indicators like Water Use Efficiency (WUE), Water Application Efficiency (WAE), and Relative Water Supply (RWS) are commonly used to quantify performance, highlighting how AWD often ensures a more resilient and sustainable balance between water use and crop demand compared to other methods [23].

2.4 Irrigation System Organization in Italy and Piemonte

In Italy, the management of irrigation and land reclamation infrastructure is entrusted to irrigation and reclamation districts, which are public legal entities with a self-governing, associative structure. Their institutional mission includes the maintenance of hydraulic safety, the provision and regulation of irrigation water, and the safeguarding of the environment and agricultural productivity. These functions are carried out through the design, construction, and management of a vast network of hydraulic infrastructures, such as canals, reservoirs, pumping stations, embankments, and water regulation structures [30].

At the national level, the National Association of Reclamation, Irrigation and Land Improvement Districts (ANBI) represents and coordinates 142 such entities. Recognized as a public-interest association since 1947, ANBI promotes sustainable land and water resource management, supports institutional dialogue, and facilitates innovation, research, and training activities across its members. Italy's district-based system covers nearly 60% of the national territory and manages more than 231,000 km of irrigation and drainage canals, as well as over 900 reservoirs, 2,000 irrigation structures, and 342 hydroelectric plants [31].

In Piedmont, the system is represented regionally by ANBI Piemonte, established in 2008 and currently composed of 25 member districts. These entities oversee water distribution and maintain irrigation infrastructure within their respective areas, which are often aligned with hydrographic basins. According to ANBI [32] data, approximately 18.3% of the regional territory is served by these districts. Their activities encompass not only irrigation but also soil conservation, landscape protection, and climate change mitigation, supporting environmental and agricultural resilience in the region.

The numerous irrigation districts (*consorzi*) vary widely in both size and organization.

They range from small-scale entities, such as Ossolano Irrigazione (2,000 ha), to large interregional organizations like the Associazione Irrigazione Est Sesia, which manages approximately 330,000 ha, with a significant portion of its jurisdiction located in neighboring Lombardy.

In the rice-growing plains of Vercelli, Novara, Biella, and Alessandria, the irrigation infrastructure is particularly developed and historically consolidated. Major districts operating in this area include the Associazione d'Irrigazione Ovest Sesia (AIOS), the Associazione Irrigazione Est Sesia, and the Consorzio di Bonifica della Baraggia Biellese e Vercellese. These areas are primarily supplied by large rivers such as the Po, Dora Baltea, Sesia, and Ticino, with total flow rates exceeding 500 m^3/s, particularly through the historic Canali Cavour system, active since the late 19th century.

In Northern Piedmont, smaller districts such as Angiono Foglietti, Canavese, and

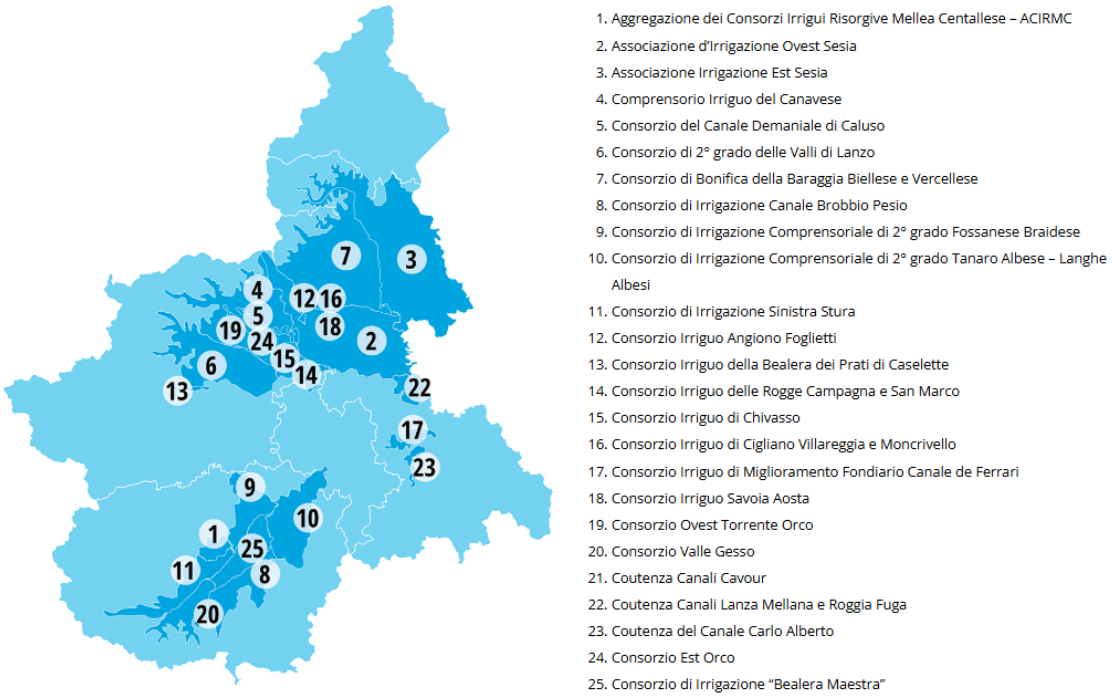

Figure 2.9: Irrigation Districts in Piemonte.

those in the Valli di Lanzo manage localized irrigation needs. These areas often rely on water lifted directly from the Dora Baltea River, and are characterized by the presence of orchards and vegetable crops. The northern and eastern parts of the region show a coexistence of small first-degree districts and large consolidated irrigation systems, heavily influenced by rice cultivation practices.

The Alessandria–Tortona plain, together with part of the Cuneo province, represents another important irrigation zone. This area benefits from Appennine river systems such as the Scrivia, Curone, Tanaro, and Bormida, and is irrigated mainly through surface irrigation systems (53%) and sprinkler systems (47%). There are 48 identified water sources, with 56% of water taken from rivers and 23% from groundwater.

The Turin area, encompassing the entire province of Torino, part of Asti, and the northeastern part of Cuneo, is rich in water resources. It includes major rivers such as the Po, Dora Baltea, Dora Riparia, Orco, Pellice, Sangone, Stura di Lanzo, Malone, and Chiosola. Here, 11 irrigation districts operate, most of them small and located in mountainous areas. Notably, the area relies heavily on surface irrigation systems (96%), and benefits from abundant precipitation and the presence of natural springs (fontanili), especially along the Pellice River. There are more than 610 identified water sources, with 61% consisting of river withdrawals and 98% of the total flow volume allocated for irrigation purposes.

In the Cuneo area (southwestern Piedmont), irrigation is managed by 16 small districts, the largest being the ACISS – Aggregazione Consorzi Irrigui Sinistra Stura di Demonte, which oversees nearly 80,000 ha. The water supply here is highly diversified

and includes torrents, wells, and small hillside reservoirs, totaling over 730 sources, of which 35% come from rivers and 33% from groundwater. The widespread use of private wells indicates a level of autonomous water management, supplementing the services provided by the public irrigation districts [32].

Chapter 3

Study Area

A detailed description of the study area is essential, as the main objective of this work is to estimate the volume of water required for irrigation. The calculation of this volume is based on the product between the Irrigation water depth estimated by the model and the corresponding agricultural surface area. It is therefore crucial to identify the extent of cultivated land, categorized by crop type, highlighting how rice represents the predominant cultivation in the area. This consideration further supports the motivation behind the present thesis. A first overview on the AIOS district and the area managed by them is given. Then an agricultural characterization is performed in order to observe the main cultivation of the area.

3.1 Study Area

This study focuses on one of the largest and most active districts in the region : Asociazione d'Irrigazione Ovest Sesia (AIOS). It covers approximately 100,000 hectares, encompassing the territories of Biella, Vercelli, and parts of the Casale Monferrato area. The water required to serve this district is withdrawn—by right or concession—from major rivers such as the Dora Baltea, Sesia, and Po, as well as from the Elvo and Cervo streams.

The consortium is primarily dedicated to providing irrigation services to around 9,000 member farms, but its role extends far beyond water distribution. AIOS is also active in soil and hydraulic defense, hydropower, environmental restoration, and territorial management. These activities are enabled by deep expertise in water regulation and the availability of a dense and historic canal network.

AIOS is composed of 59 irrigation districts, each governed by its own locally elected administration. These districts operate under the coordination and technical oversight of the General Directorate. In addition to districts, the consortium also includes "Tenimenti Isolati" (individual large-scale properties managed independently) and zones served by "Luci Libere", where irrigation is directly handled by the central administration due to the absence of district-level organization [33].

The consorzio manages a vast and intricate irrigation network composed of over 1,100 flow regulation structures (modulators), monitored daily by on-site operators (acquaioli).

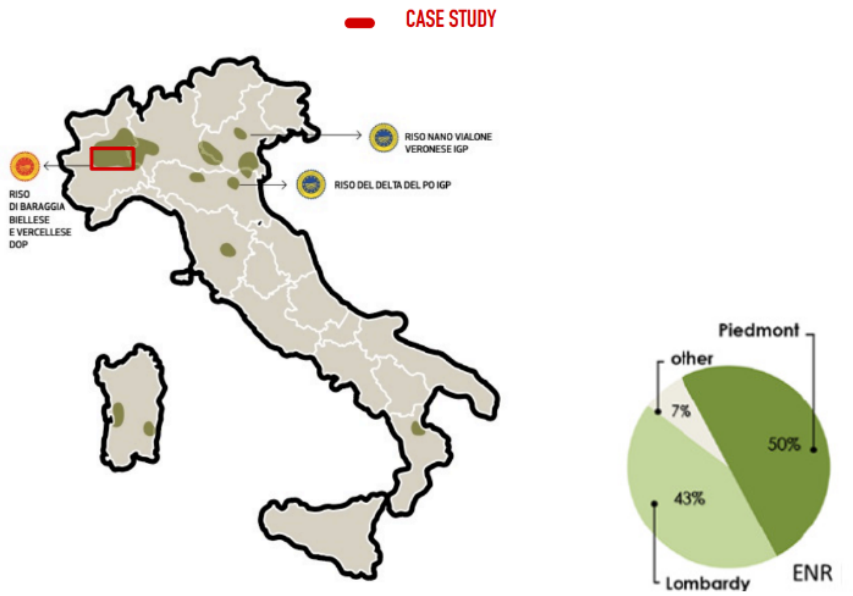

Figure 3.1: General overview on main rice-cultivate area in Italy and the identification of the pilot district of the sudy..

The main irrigation channels—such as the Cavour Canal, Naviglio d'Ivrea, Canale Depretis, and Roggia Marchesa—draw water from multiple rivers and streams to distribute it across the region.

The irrigation method is primarily gravity-fed surface irrigation and submersion, taking advantage of the region's natural slope and soil permeability. Water applied to fields is reused both:

- superficially, as runoff is collected into drainage channels ("colatori") and reused downstream;
- and subsurface, as infiltrated water recharges the aquifer, eventually reemerging in natural springs (fontanili).

The network reaches full operational capacity by May, with the irrigation season running from late March to September.

The AIOS manages canals west of the Sesia River, while its counterpart, the Associazione Irrigazione Est Sesia, oversees the eastern portion. Shared channels serving both districts are jointly managed by the Coutenza Canali Cavour, a cooperative body established in 1978.

3.2 Data Source

The data used in this Study area characterization phase originate from official regional sources in the Piedmont Region. The main sources consulted are:

- SIBI project for the delimitation of irrigation district [34].
- The Piedmont Geoportal for data on Utilized Agricultural Area - SAU [35].
- The official website of AIOS [33] was consulted to validate the data retrieved from the Geoportal and to gather descriptive information about the study area.

Regarding the spatial delimitation of irrigation districts in Piedmont, the *Sistema Informativo della Bonifica ed Irrigazione (SIBI)* – established by Regional Law 21/1999 – was consulted. SIBI aims to collect, process, and disseminate information, including cartographic data, related to land reclamation and irrigation infrastructure across the region. It provides an updated overview of irrigation works managed by consortia, describes the physical characteristics of the land, and supports the development and implementation of regional plans and programs. This project is part of a broader national initiative promoted by the Italian Ministry of Agriculture (MIPAAF) and managed by CREA, through the National Information System for the Management of Water Resources in Agriculture (SIGRIAN). For this thesis, several shapefile datasets derived from SIBI were used. Since SIBI is an evolving project, some information may be partially inaccurate. The information used in this work were updated as of January 2025. After comparing it with the information available on the AIOS website [33], the spatial boundaries of the consortium were found to be accurate.

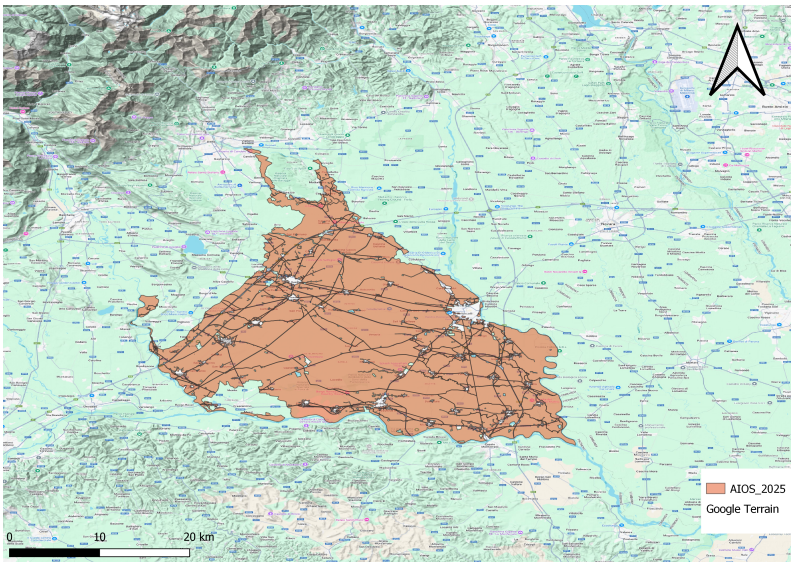

Figure 3.2: AIOS shape file from SIBI updated as of january 2025.

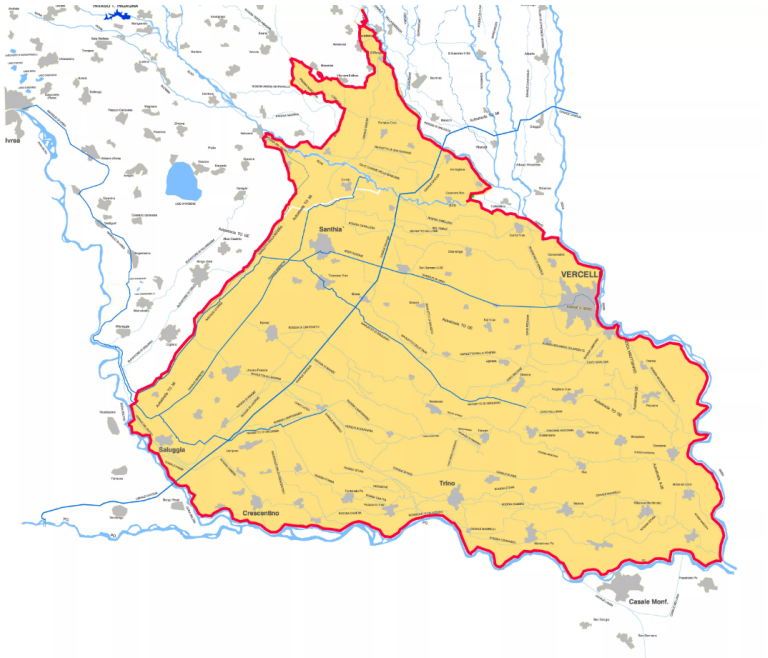

Figure 3.3: AIOS map from the official website.[33]

The data regarding the Utilized Agricultural Area (SAU), arranged by crop type, were extracted from the *GeoPortale Piemonte* [35]. This platform is the official tool through which the Piedmont Region promotes access to, sharing of, and harmonization of geographic data.

The datasets used for this thesis are drawn from the "Agricultural Land Use on the

Regional Cadastre Mosaic – 2022 and 2023", which provides detailed parcel-level information on predominant agricultural land use. This dataset is part of the Cadastre Mosaic Project, developed through the processing of cadastral information available from the SigmaTer exchange system, and referenced in the *WGS84/UTM 32N* cordinate system.

The determination of predominant land use for each parcel follows a hierarchical system based on three criteria:

- By Predominant Crop: the crop occupying more than 50% of the parcel's area is selected;
- By Standard Output (SO): if no crop exceeds the 50% threshold, the one with the highest SO is chosen;
- By regional priority: if no crop is predominant by area or SO (e.g., in the case of crops with similar SO values), the crop considered most relevant for the Piedmont Region is selected.

The Standard Output (SO) represents the potential gross output of agricultural holdings and is calculated for each crop and region using standard average values.

Each parcel is first classified into three main categories: arable land, meadows and pastures, and permanent crops. Each of these categories is then further subdivided into multiple levels, down to the specific crop type.

The spatial datasets used in this study, once collected from various institutional sources, were managed, processed, and visualized using QGIS, an open-source Geographic Information System widely adopted in the fields of territorial management and environmental analysis.

By intersecting the shapefile of the areas managed by AIOS with the crop data from the Geoportal, the Utilized Agricultural Area (UAA) was obtained for the analyzed territory, broken down by crop type for the years 2021, 2022 and 2023.

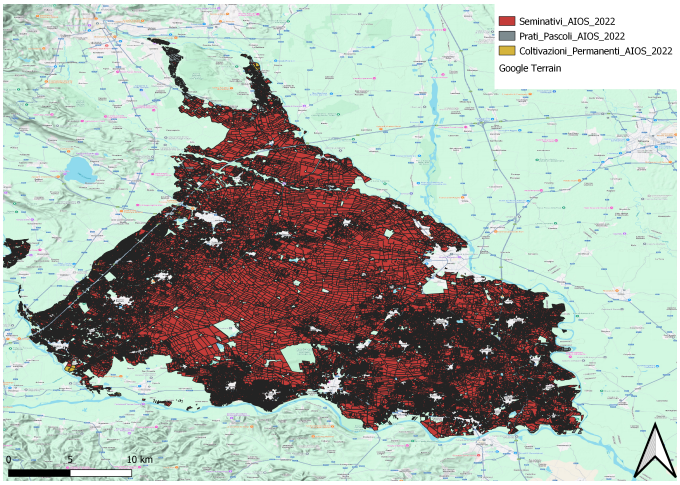

Figure 3.4: Utilized Agricultural Area (UAA) within the AIOS district for the year 2022, classified into three main categories.

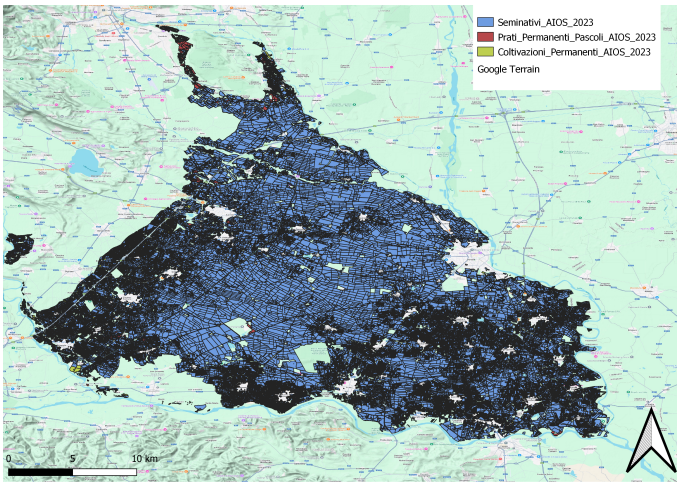

Figure 3.5: Utilized Agricultural Area (UAA) within the AIOS district for the year 2023, classified into three main categories.

Then for each crops some information were extracted, calculated and organized in tables using Microsoft Excel. The crop tables mainly include the corresponding surface areas. The aim was to quantify the total area occupied by each crop and to observe inter-annual variations as a potential response to climatic conditions and variation in the Agricultural and Irrigation management system. Then some key statistical metrics such as the maximum, minimum, and average size of cultivated parcels for each crop type were computed. These indicators serve as a foundation for understanding the spatial distribution of crops and for characterize the area.

3.3 Characterization of Cultivated Areas and Statistical Indicators

This paragraph presents the results of the statistical analysis carried out to characterize the territory and obtain information on the cultivated areas for each crop type, which will later be used to estimate the irrigation volumes for the region. The analyses focused on several key elements:

- Types of crops present;
- Calculation of area occupied by only rice in 2021
- Calculation of the areas occupied by each crop in 2022 and 2023 to perform then a district characterization and interannual variability assessment;
- Top 10 crops by utilized area;
- Analysis of area variations between the two years;
- Minimum, maximum, and average size of cadastral parcels for each crop;

The characterization of the area was derived from the cadastral parcel data processed through the regional geoportal and includes all crop types identified within the district boundaries. The resulting crop typology reflects the diversity and complexity of agricultural use in the area, encompassing cereals, legumes, forage crops, industrial and permanent crops, as well as vegetables and orchards.

The following table presents the complete list of crops identified in both years (22/23). Crops that appear in only one of the two years are explicitly marked, providing an initial indication of interannual variability in land use.

To quantitatively assess the distribution of agricultural land use within the AIOS irrigation district, a detailed analysis of the surface areas occupied by each crop type was carried out for the years 2022 and 2023. The calculation was performed using QGIS, applying the `Aggregate` function on the intersected cadastral parcels. This tool allowed for the summation of parcel areas grouped by crop code, thereby generating the total utilized surface per crop. For 2021 only the total area occupied by rice was extracted.

The input dataset was the regional land use map extracted from the GeoPortale Piemonte, previously intersected with the spatial boundaries of the AIOS district. All crop categories identified in the source dataset were included, covering a wide range of annual and permanent crops, meadows, pastures, fallow land, and nurseries.

The full results for 2022-2023 period of this analysis are reported in Table 3.2. The table lists, for each crop type, the total cultivated surface in hectares for the two years considered, along with the absolute and percentage variation between 2022 and 2023. The comparison focused on this two years since it was pretty interesting to observe the agricultural variation after a critical year as it was 2022. However also area statistics for 2021 were extracted and used later in the study.

Crop Types	Crop Types
N.D.	ACTINIDIA
ALBICOCCO	ALTRA FRUTTA TEMPERATA
ALTRE ORTIVE DI PIENO CAMPO	ALTRE ORTIVE IN ORTI STAB. O IND.
ALTRI CEREALI	ALTRI ERBAI
ALTRI ERBAI MONOFITI DI CEREALI	ALTRI LEGUMI SECCHI
ALTRI PRATI AVVICENDATI	AVENA
CASTAGNO	CILIEGIO
COLZA E RAVIZZONE	ERBA MEDICA
FAVA	FIORI E PIANTE ORNAMENTALI IN PIENA ARIA
FIORI PROTETTI IN SERRA	FRUMENTO DURO
FRUMENTO TENERO E SPELTA	GIRASOLE
GRANTURCO	GRANTURCO MATURAZIONE CEROSA
GRANTURCO IN ERBA	MELO
NETTARINA	NOCCIOLO
NOCE	ORZO
PASCOLI	PATATA
PERO	PESCO
PIANTE AROMATICHE, MEDICINALI E COND.	PISELLO SECCO
PRATI PERMANENTI	RISO
SOIA	SORGO
SUSINO	TERRENI A RIPOSO, SENZA AIUTO
VITE	VIVAI, ALTRI
VIVAI, FRUTTIFERI	VIVAI, PIANTE ORNAMENTALI
SEMENTI	FAGIUOLI SECCHI
POMODORO DA MENSA	

Table 3.1: Crop types identified in the AIOS district for the years 2022 and 2023. Crops highlighted in red appear only in 2022; those in green only in 2023.

Crop Type	2022 (ha)	2023 (ha)	Variation (ha)	% Variation
ACTINIDIA	102.17	86.49	-15.68	-15.35
ALBICOCCO	0.99	0.99	0.00	0.00
ALTRA FRUTTA TEMPERATA	8.57	9.06	0.50	5.79
ALTRE ORTIVE DI PIENO CAMPO	60.52	103.50	42.98	71.01
ALTRE ORTIVE IN ORTI STAB. O IND.	47.98	55.29	7.30	15.22
ALTRI CEREALI	268.68	276.22	7.54	2.81
ALTRI ERBAI	1051.45	705.32	-346.13	-32.92
ALTRI ERBAI MONOFITI DI CEREALI	318.18	793.68	475.51	149.45
ALTRI LEGUMI SECCHI	1.72	0.43	-1.29	-74.80
ALTRI PRATI AVVICENDATI	797.89	695.92	-101.97	-12.78
AVENA	7.33	10.82	3.50	47.69
CASTAGNO	13.35	13.77	0.42	3.18
CILIEGIO	2.05	2.35	0.30	14.45
COLZA E RAVIZZONE	136.83	131.49	-5.34	-3.90
ERBA MEDICA	104.23	65.83	-38.40	-36.84
FAGIUOLI SECCHI	0.00	15.78	15.78	0.00
FAVA	30.01	1.72	-28.29	-94.28
FIORI E PIANTE ORNAMENTALI IN PIENA ARIA	0.64	0.18	-0.46	-72.37
FIORI PROTETTI IN SERRA	1.26	1.26	0.00	0.00
FRUMENTO DURO	7.11	14.43	7.32	102.93
FRUMENTO TENERO E SPELTA	1152.73	1912.50	759.77	65.91
GIRASOLE	71.97	52.70	-19.28	-26.78
GRANTURCO	8854.58	8398.26	-456.32	-5.15
GRANTURCO A MATURAZIONE CEROSA	1346.97	1203.06	-143.90	-10.68
GRANTURCO IN ERBA	377.27	453.90	76.64	20.31
MELO	64.91	49.19	-15.72	-24.21
NETTARINA	1.74	1.25	-0.49	-27.93

Table 3.2: Total cultivated area by crop type in 2022 and 2023 within the AIOS district.

Crop Type	**2022 (ha)**	**2023 (ha)**	**Variation (ha)**	**% Variation**
NOCCIOLO	29.06	29.06	0.00	0.00
NOCE	49.01	49.01	0.00	0.00
ORZO	594.73	784.82	190.10	31.96
PASCOLI	96.14	70.60	-25.54	-26.57
PATATA	2.30	1.97	-0.34	-14.65
PERO	7.08	7.08	0.00	0.00
PESCO	27.98	27.41	-0.57	-2.02
PIANTE AROMATICHE, MEDICINALI E COND.	3.14	2.01	-1.13	-36.09
PISELLO SECCO	38.66	19.71	-18.95	-49.02
POMODORO DA MENSA	0.00	21.45	21.45	0.00
PRATI PERMANENTI	651.58	511.04	-140.54	-21.57
RISO	60192.35	60345.06	152.71	0.25
SEMENTI	12.34	0.00	-12.34	-100.00
SOIA	2774.71	2327.88	-446.83	-16.10
SORGO	3.07	6.93	3.87	126.15
SUSINO	1.71	1.71	0.00	0.00
TERRENI A RIPOSO, SENZA AIUTO	519.87	359.74	-160.13	-30.80
VITE	11.89	11.07	-0.82	-6.92
VIVAI, ALTRI	14.08	14.89	0.80	5.71
VIVAI, FRUTTIFERI	0.72	0.72	0.00	0.23
VIVAI, PIANTE ORNAMENTALI	2.48	4.71	2.23	89.64
ND	155.85	93.71	-62.14	-39.87
TOTALE	80058.10	79718.11	-339.99	-0.42

Table 3.2: Total cultivated area by crop type in 2022 and 2023 within the AIOS district.

To better identify dominant land uses and prioritize irrigation demand modeling, the ten most extensive crops in 2022 and 2023 were extracted and are summarized in tables below:

Crop Type	**2022 Surface (ha)**
RISO	60192.35
GRANTURCO	8854.58
SOIA	2774.71
GRANTURCO A MATURAZIONE CEROSA	1346.97
FRUMENTO TENERO E SPELTA	1152.73
ALTRI ERBAI	1051.45
ALTRI PRATI AVVICENDATI	797.89
PRATI PERMANENTI	651.58
ORZO	594.73

Table 3.3: Top 10 crops by cultivated area in 2022 within the AIOS district.

Crop Type	**2023 Surface (ha)**
RISO	60345.06
GRANTURCO	8398.26
SOIA	2327.88
FRUMENTO TENERO E SPELTA	1912.50
GRANTURCO A MATURAZIONE CEROSA	1203.06
ALTRI ERBAI MONOFITI DI CEREALI	793.68
ORZO	784.82
ALTRI ERBAI	705.32
ALTRI PRATI AVVICENDATI	695.92

Table 3.4: Top 10 crops by cultivated area in 2023 within the AIOS district.

The graphs highlight the ten most extensive crops, or categories of agricultural land use, within the AIOS irrigation district, based on total cultivated area (expressed in hectares). In both years analyzed, 2022 and 2023, rice clearly stands out as the dominant crop, accounting for approximately 75% of the total utilized agricultural area. This figure underscores the strategic importance of rice in the region, not only because of its widespread cultivation but also due to its exceptionally high irrigation demand, making it a central focus in the context of irrigation modeling.

Maize, soybean, soft wheat, and various types of temporary or rotational meadows follow rice in terms of cultivated area. While some minor variations in crop ranking and surface extent are observed between the two years, likely due to crop rotation practices, seasonal climatic conditions, or market dynamics, the overall agricultural structure remains relatively stable over time.

A particularly relevant insight emerges from the cumulative distribution curve. Although the dataset includes more than 45 distinct crop types or land-use categories, the top ten alone account for nearly 98% of the total cultivated area. This highlights how irrigation demand is almost entirely concentrated within a limited number of dominant crops. From a planning and management perspective, this concentration offers a significant operational advantage, as it allows efforts and resources to be directed toward those crops that effectively determine the vast majority of water demand across the district.

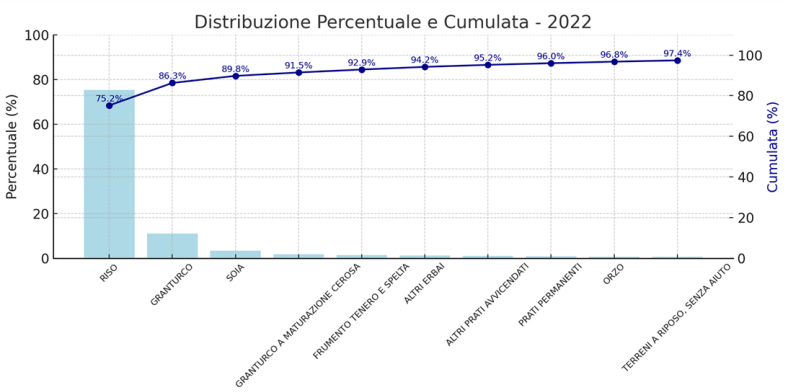

Figure 3.6: Percentage and cumulative distribution of cultivated area by crop type in 2022 within the AIOS district.

While the overall crop distribution has remained largely consistent, annual fluctuations can be seen in the table and they can provide insights into how external factors, such as climate conditions or market dynamics, may have influenced agricultural decisions.

The following table summarizes the total surface variation between the two years for the top ten crops previously identified. These data allow for a more in-depth understanding of temporal dynamics in land use and may help identify potential links between environmental factors and agricultural planning.

Crop	**2022**	**2023**	**Δ ha**	**Δ %**
RISO	60192	60345	153	0.0
GRANTURCO	8855	8398	-456	-5.0
SOIA	2775	2328	-447	-16.0
GRANTURCO A MATURAZIONE CEROSA	1347	1203	-144	-11.0
FRUMENTO TENERO E SPELTA	1153	1912	760	66.0
ALTRI ERBAI	1051	705	-346	-33.0
ALTRI PRATI AVVICENDATI	798	696	-102	-13.0
PRATI PERMANENTI	652	511	-141	-22.0
ORZO	595	785	190	32.0
TERRENI A RIPOSO, SENZA AIUTO	520	360	-160	-31.0
TOTALE	80058	79718	-340	-0.4

Table 3.5: Variation of cultivated areas (ha) between 2022 and 2023 for the ten most extensive crop types, including fallow land.

The total cultivated surface shows a slight decrease of approximately 340 hectares from 2022 to 2023, corresponding to a reduction of about 0.4%. While this may seem marginal, it could represent a symptom of broader stressors on the agricultural system. Annual climatic reports from regional sources such as ARPA indicate that 2022 was the hottest year on record and the second driest since 1958 [36]. Such extreme conditions could plausibly account for both the reduction in total cultivated area and the variations observed in specific crop types. Examining individual crops reveals a more detailed picture. Despite the overall decline, rice, by far the most important crop in terms of surface area, experienced a slight increase of about 0.25%. This result is particularly relevant given that rice is an extremely water-intensive crop, and its expansion ,even after one of the driest year, reinforces its strategic and economic importance in the region and highlights the district's structural dependence on this crop, which plays a key role in both land use and irrigation resource planning. Other crops, such as maize and soybean, experienced more substantial reductions in area, likely due to their lower economic priority or higher sensitivity to adverse weather. Meanwhile, crops such as soft wheat and barley saw moderate increases, potentially reflecting more flexible crop rotation strategies or a better adaptation to local conditions.

Afterward, statistical metrics regarding the minimum, average, and maximum parcel

size were extracted for each crop type. These statistics are not just technical data, but provide essential insights into different aspects of the agricultural structure of the area. Larger fields, for instance, tend to allow for more mechanized and efficient farming practices, which directly affects both productivity and resource management. Additionally, parcel size can reflect the level of crop diversification, and it may influence the choice of irrigation systems, with certain techniques being more suitable depending on the scale of the field. A first analysis in table 3.6 includes all crop types and shows that some minor crops in terms of total area, such as walnut, rapeseed, dry peas, pear, fava bean, and apple, rank among the top for average or maximum parcel size. However, this result is often biased by the presence of just one or a few very large parcels, which heavily influence the average values. For this reason, these tables must be interpreted with caution, especially for crops with very limited total surface area.

To address this, a more meaningful representation is shown in Figure 3.7, where a box plot is used to visualize the distribution of parcel sizes for the top ten crops by total cultivated area. This allows for a better understanding of the actual variability and typical size ranges, minimizing the effect of outliers.

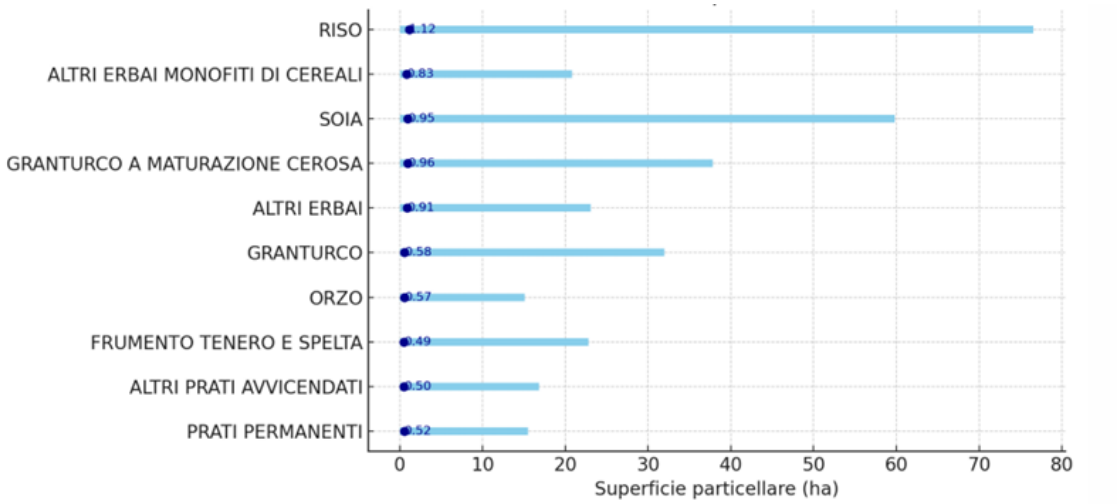

Figure 3.7: Box Plot parcel size for the 10 main crops of the area.

From the box plot, it becomes clear that crops such as rice, maize, and soft wheat not only dominate in terms of total area but also show consistently large parcel sizes. Rice, in particular, stands out with maximum values approaching 80 hectares, confirming its strategic importance for the region, especially in light of its high irrigation demands. In this case, the high maximum values do not distort the average figures significantly due to the crop's widespread distribution and volume. This reinforces the idea that irrigation planning and sustainable water use strategies should be focused primarily on these dominant crops and especially rice.

Crop Type	Max (2022)	Min (2022)	Mean (2022)	Max (2023)	Min (2023)	Mean (2023)
N.D.	10.46	0.0	0.5	7.83	0.0	0.32
ACTINIDIA	3.87	0.0	0.5	3.87	0.0	0.5
ALBICOCCO	0.56	0.18	0.33	0.56	0.18	0.33
ALTRA FRUTTA TEMPERATA	0.66	0.08	0.36	0.66	0.08	0.36
ALTRE ORTIVE DI PIENO CAMPO	2.63	0.01	0.39	13.72	0.02	0.65
ALTRE ORTIVE IN ORTI STAB. O IND.	2.1	0.07	0.38	3.08	0.02	0.44
ALTRI CEREALI	13.72	0.0	0.63	7.82	0.0	0.67
ALTRI ERBAI	23.08	0.0	0.91	12.3	0.0	0.65
ALTRI ERBAI MONOFITI DI CEREALI	20.78	0.01	0.83	20.44	0.0	0.9
ALTRI LEGUMI SECCHI	1.72	1.72	1.72	0.43	0.43	0.43
ALTRI PRATI AVVICENDATI	16.8	0.0	0.5	16.8	0.0	0.5
AVENA	2.23	0.2	1.05	10.38	0.16	3.61
CASTAGNO	1.14	0.02	0.38	1.14	0.02	0.37
CILIEGIO	1.0	0.09	0.41	1.0	0.08	0.34
COLZA E RAVIZZONE	45.98	0.03	1.87	26.3	0.02	0.91
ERBA MEDICA	13.79	0.0	0.49	3.95	0.0	0.41
FAVA	12.3	0.11	2.73	0.9	0.41	0.57
FIORI E PIANTE ORNAMENTALI IN PIENA ARIA	0.18	0.1	0.13	0.18	0.18	0.18
FIORI PROTETTI IN SERRA	0.54	0.03	0.32	0.54	0.03	0.32
FRUMENTO DURO	3.2	0.14	0.79	1.45	0.01	0.22
FRUMENTO TENERO E SPELTA	22.77	0.0	0.49	45.98	0.0	0.52
GIRASOLE	2.59	0.1	0.5	10.46	0.07	0.49
GRANTURCO	31.97	0.0	0.58	32.03	0.0	0.59
GRANTURCO A MATURAZIONE CEROSA	37.84	0.01	0.96	37.84	0.01	0.84
GRANTURCO IN ERBA	13.55	0.0	0.68	20.78	0.0	0.84
MELO	16.81	0.06	0.97	5.91	0.06	0.73
NETTARINA	0.38	0.05	0.22	0.38	0.16	0.25
NOCCIOLO	3.83	0.0	0.38	3.83	0.0	0.38
NOCE	18.89	0.14	4.46	18.89	0.14	4.46
ORZO	15.11	0.0	0.57	15.78	0.0	0.57
PASCOLI	8.62	0.0	0.57	8.62	0.0	0.58
PATATA	0.46	0.12	0.23	1.09	0.12	0.39
PERO	5.24	0.21	1.42	5.24	0.21	1.42
PESCO	1.17	0.09	0.31	1.17	0.09	0.32
PIANTE AROMATICHE, MEDICINALI E COND.	0.79	0.0	0.21	0.55	0.17	0.4
PISELLO SECCO	6.37	0.12	0.69	3.64	0.07	1.1
PRATI PERMANENTI	15.47	0.0	0.52	11.49	0.0	0.45
RISO	76.55	0.0	1.12	76.55	0.0	1.13
SOIA	59.79	0.0	0.95	59.79	0.0	0.85
SORGO	0.36	0.08	0.22	1.31	0.09	0.3
SUSINO	0.71	0.25	0.43	0.71	0.25	0.43
TERRENI A RIPOSO, SENZA AIUTO	16.95	0.0	0.56	12.24	0.0	0.42
VITE	0.76	0.03	0.28	0.73	0.03	0.27
VIVAI, ALTRI	0.77	0.01	0.24	1.45	0.01	0.28
VIVAI, FRUTTIFERI	0.72	0.72	0.72	0.72	0.0	0.36
VIVAI, PIANTE ORNAMENTALI	0.82	0.01	0.25	0.82	0.01	0.21
SEMENTI	15.1	0.01	0.87	0.0	0.0	0.0
FAGIUOLI SECCHI	0.0	0.0	0.0	1.83	0.04	0.58
POMODORO DA MENSA	0.0	0.0	0.0	0.03	0.03	0.03

Table 3.6: Parcel size statistics (minimum, average, and maximum in hectares) for each crop in 2022 and 2023.

Chapter 4

Materials and Methods

This chapter describes the methodological approach adopted for the quantification of the irrigation requirements of rice in the study area. The objective is to provide a clear and systematic description of the procedures followed, in order to ensure both the transparency and the reproducibility of the work carried out.

In particular, after presenting the input data used (climatic, soil and crop-related), the structure of the water balance model is illustrated. The model was originally developed starting from Rolle's [10] formulation and subsequently adapted to the specific needs of rice cultivation. The implementation of the model is then described, both at point scale and at spatial scale, together with the procedures for data processing through computational tools and GIS.

The chapter concludes with the presentation of the simulated irrigation strategies, which include both the traditional practice of continuous flooding (CF) and the innovative and water saving approaches of Alternate Wetting and Drying (AWD) and Dry seeding with late flooding (DFL).

4.1 Input Data

4.1.1 Climatic Data

In this work, climate input data were obtained from the *ERA5 downscaling @2.2 km over Italy* dataset, produced by the **Centro Euro-Mediterraneo sui Cambiamenti Climatici** (CMCC). This product provides high-resolution reanalysis fields resulting from the dynamical downscaling of the ERA5 dataset, originally available at a horizontal resolution of about 31 km $\times$ 31 km, to a finer grid of 2.2 km $\times$ 2.2 km. The downscaling procedure was carried out specifically for the project (foreground) using the Regional Climate Model (RCM) *COSMO5.0_CLM9* in combination with *INT2LM 2.06* [37].

Reanalysis data offer a spatially and temporally consistent reconstruction of past atmospheric conditions by combining observations from multiple sources (e.g., satellite, ground-based, and other in situ measurements). Among them, ERA5 represents the latest global reanalysis developed by the *European Centre for Medium-Range Weather Forecasts* (ECMWF), providing hourly estimates of a wide range of atmospheric, land-surface, and

oceanic variables, together with associated uncertainty information [38].

The dataset spans the period from 1 January 1981 00:00 to 31 December 2023 23:00, with a temporal resolution of one hour. Consequently, the hourly data from the employed dataset were aggregated to a daily scale. The main climatic variables used as input for the sub–soil water balance model are **precipitation (P)** and **reference evapotranspiration ($\mathbf{ET_0}$)**, both available at a hourly temporal resolution, in a period that ranges from 2018 to 2022.

The reference evapotranspiration (expressed in mm day^{-1}) was estimated using the **Hargreaves–Samani method**, as already described in Chapter 2. The daily reference evapotranspiration, $ET_{0,i}$, for day i is computed as:

$$ET_{0,i} = k_{HS} \times R_{a,i} \times (T_{mean,i} + 17.8) \times \sqrt{T_{max,i} - T_{min,i}} \tag{4.1}$$

where:

- i is the specific day of the analysis;
- $T_{max,i}$, $T_{min,i}$, and $T_{mean,i}$ are respectively the maximum, minimum, and mean daily air temperatures [°C];
- $R_{a,i}$ is the equivalent evaporation [mm], obtained by dividing the top–of–atmosphere solar radiation by the latent heat of vaporization of water ($1/\lambda = 0.408$);
- k_{HS} is an empirical coefficient.

The empirical coefficient k_{HS} was initially set to a fixed value of 0.0023, as proposed in the original formulation by Hargreaves and Samani. However, a **spatial variability of** k_{HS} was introduced to improve the accuracy of ET_0 estimation across different climatic regions. Specifically, k_{HS} values were derived by multiplying the constant 0.0023 by the ratio between the annual reference evapotranspiration computed using the Penman–Monteith (PM) and Hargreaves–Samani (HS) methods.

4.1.2 Soil Data

The soil data used in this study were derived from the **SoilGrids** database. It is a global digital soil mapping system that combines worldwide soil profile information with a set of environmental covariates to model the spatial distribution of soil properties across the globe. It provides global soil property maps generated using **machine learning algorithms** at a spatial resolution of 250 m, with predictions available for six standard soil depth intervals.The system employs global models calibrated using all available soil profile observations and globally accessible environmental covariates, ensuring spatially consistent predictions without discontinuities across national boundaries. Layers are produced through a **reproducible digital soil mapping workflow**, which enables regular updates whenever new soil data or covariates become available, following data quality control and harmonization procedures. SoilGrids is developed and maintained by **ISRIC – World Soil Information**, within the framework of international scientific collaboration [39].

In this study, soil property data were extracted specifically for the **percentage content of clay and sand**. For both variables, values corresponding to the 0–5 cm and 5–15 cm depth layers were retrieved and subsequently averaged to characterize the **topsoil layer**. The resulting soil property maps were **resampled and spatially adjusted** to match the resolution and grid of the CMCC dataset used for the climatic variables.

The **ISRIC SoilGrids250m** product serves as the foundation and input data source for **HiHydroSoil**, a global database of soil hydraulic properties developed by *FutureWater* [40]. HiHydroSoil represents the dataset used in this study for hydraulic data. It provides a wide range of hydraulic parameters, as illustrated in the figure below 4.1.

Name	Variable	Unit
ORMC	Organic Matter Content	%
STC	Soil Texture Class	O (Organic), VF (Very Fine), F (Fine), MF (Medium Fine), C (Coarse), M (Medium)
ALPHA	Alpha parameter for Mualem Van Genuchten Equation	1/cm
N	N parameter for Mualem Van Genuchten Equation	-
WCsat	Saturated Water Content	m^3/m^3
WCres	Residual Water Content	m^3/m^3
Ksat	Saturated Hydraulic Conductivity	cm/d
WCpF2	Water content at pF2 (field capacity)	m^3/m^3
WCpF3	Water content at pF3 (critical point)	m^3/m^3
WCpF4.2	Water content at pF4.2 (permanent wilting point)	m^3/m^3
WCavail	Available water content	m^3/m^3
SAT-FIELD	Water content between saturation point and field capacity (pF2)	m^3/m^3
FIELD-CRIT	Water content between field capacity (pF2) and critical point (pF3)	m^3/m^3
CRIT-WILT	Water content between critical point (pF3) and permanent wilting point (pF4.2)	m^3/m^3
Hydrologic_Soil_Group	Hydrologic Soil Group	A (low runoff potential), A/D, B (moderately low runoff potential), B/D, C (moderately high runoff potential), C/D, D (high runoff potential)

Figure 4.1: Soil hydraulic properties included in the HiHydroSoil v2.0 database. [40]

The hydraulic soil variables downloaded and used for this study are: **Water content at saturation, at field capacity and at wilting point**.

4.1.3 Crop Parameters

Crucial information related to average sowing and harvesting date in the studied district as well as biometric parameters (e.g root depth, crop height), values of crop and basal crop coefficients and the vegetation fraction cover used in this work were obtained from three main sources: (i) literature and analogous studies carried out in similar agro-climatic contexts [41], (ii) data and information from work carried out within the framework of the SPHERE project and are based, as much as possible, on values calibrated at the

regional scale and (iii) directly indications from AIOS technicians. In particular, the following coefficients were used (Tab. 4.1). The table summarizes the crop coefficients and fractional coverage parameters adopted in the model, along with the fixed root zone depths.

Table 4.1: Summary of coefficients and parameters adopted in the model.

Parameter	**Value**	**Description**
$K_{cb,ini}$	0.7	Basal crop coefficient during initial stage
$K_{cb,mid}$	1.15	Basal crop coefficient during mid-season
$K_{cb,end}$	0.7	Basal crop coefficient during late season
$K_{c,ini}$	0.9	Single crop coefficient during initial stage
$K_{c,mid}$	1.15	Single crop coefficient during mid-season
$K_{c,end}$	0.9	Single crop coefficient during late season
$K_{c,max}$	1.15	Maximum single crop coefficient
$f_{c,ini}$	0.1	Fractional cover at the beginning of the season
$f_{c,mid}$	0.9	Fractional cover at mid-season
$f_{c,end}$	0.1	Fractional cover at the end of the season
$Z_{r,min}$	0.15 m	Minimum root zone depth
$Z_{r,max}$	0.5 m	Maximum root zone depth

Considering that typical rice sowing dates in Northern Italy are concentrated between late April and early May, and assuming an average crop cycle duration of 150 days, the sowing date was set to **April 25**, while the harvest date was fixed at **September 25**.

The entire growing season was divided into four main stages: *initial stage*, *development stage*, *mid-season stage*, and *end-season stage*. Based on both local and international references, the duration of each stage was defined as follows: Dini = 31 , Ddev = 30 , Dmid = 61 , and Dend = 31 days.

These values were established by integrating the recommendations of the **FAO**[11], which suggests a general subdivision of 30-30-60-30 for a 150-day crop cycle, with local information provided by technical documents of **Ente Nazionale Risi**[42].

The **initial stage** corresponds to the period from sowing to the beginning of tillering, lasting about the first 30 days. The **development stage** represents the tillering phase, covering the following 30 days.

According to the FAO, the **mid-season stage** begins with effective full canopy cover, which occurs when the *Leaf Area Index (LAI)* reaches a value of three. The LAI is defined as the ratio between the total one-sided leaf area and the unit ground surface area. Several studies conducted in the study area [43] [44] indicate that an LAI value of three is typically reached between late June and early July, confirming the consistency of the chosen timing.

Consequently, the mid-season stage begins approximately 61 days after sowing, coinciding with the stem elongation phase, and lasts for about 60 days, as suggested by FAO.

This stage encompasses the phases of stem elongation, panicle initiation, and milk ripening, extending approximately until the **wax ripening stage**, which usually corresponds to the period when fields are gradually drained. Finally, the **end-season stage** lasts for about 31 days, covering the period from wax ripening and physiological maturity up to the final harvest.

4.2 Model structure

To estimate the irrigation water requirements of rice within the study area, a **soil water balance model** was developed by adapting and improving the methodology previously proposed by Rolle et al [10]. The model performs a **daily soil water balance** based on climatic, soil, hydraulic, and crop data, coupled with vegetation dynamics allowing continuous monitoring of the field's water status in terms of **soil moisture** and **water level**. The soil water content and level from the previous day are updated each day by integrating the incoming water inputs (precipitation and irrigation) and subtracting the daily water losses due to **actual evapotranspiration** (ET_a) and **percolation** from the balance, yielding updated end–of–day soil moisture conditions. It is therefore necessary to describe how the model manages and computes **water inputs and losses**. Regarding **water inputs** (precipitation and irrigation) distribution in the soil, the model follows the conceptual logic of a *water bucket model*. When a water input occurs, starting from completely dry conditions and considering the soil divided into two layers (*topsoil* and *subsoil*) as already described in chapter 2, the **topsoil layer** is filled first, up to its **field capacity (FC)**. Once the topsoil reaches field capacity, the **subsoil layer** begins to fill untill it reaches saturation. Any excess water beyond the saturation in the subsoil, it is then used to bring topsoil from field capacity to saturation. When both soil layers are saturated, any further incoming water contributes to the formation of a **ponded water layer** above the soil surface.

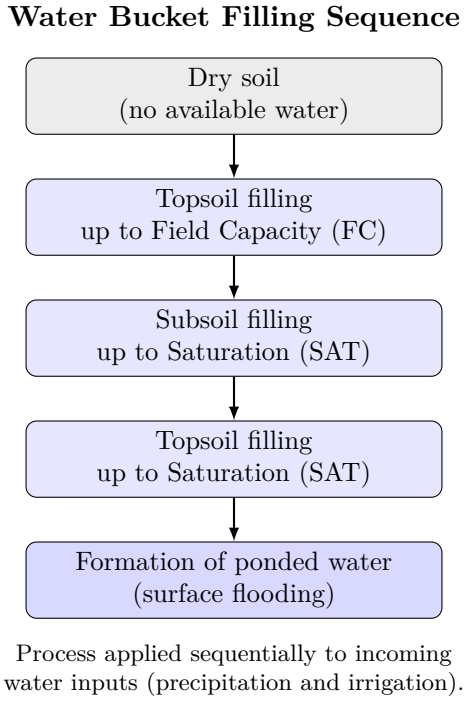

Figure 4.2: Schematic representation of the water bucket filling logic used in the model.

Regarding losses, since irrigated fields are generally almost flat, surface runoff and lateral groundwater flow within the root zone were considered negligible.

Concerning losses by evapotranspiration, it is necessary to perform a further step. Rice, being a semi–aquatic crop, starts its cycle under initial soil moisture conditions that may range from *saturated or flooded* to *relatively dry*, depending on the adopted irrigation strategy.

Given the unique behavior of rice as a flooded crop, the model distinguishes between two main hydrological phases:

1. a **ponding phase**, characterized by the presence of ponded water;
2. a **no ponding phase**, during which the water level drops below the soil surface and the subsoil begins to dry out.

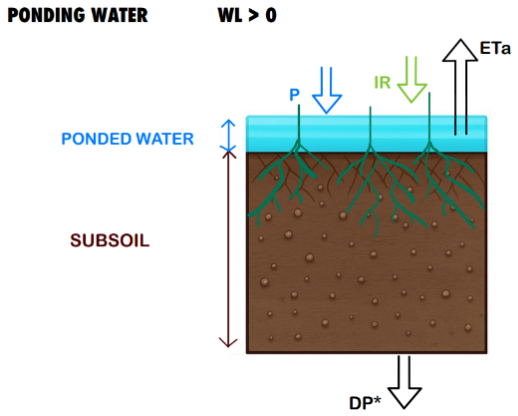

Figure 4.3: Schematic representation of a volume of soil during flooded condition. P indicates precipitation; IR irrigation; ETa actual evapotranspiration.

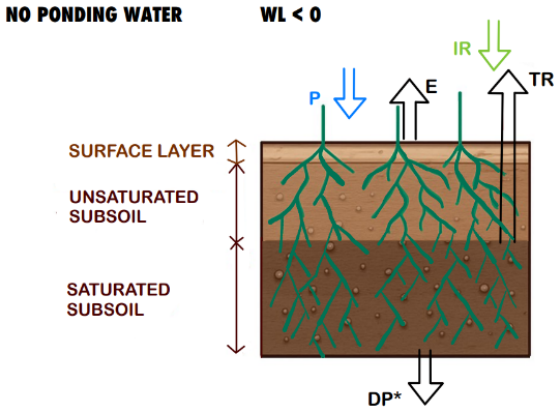

(a)

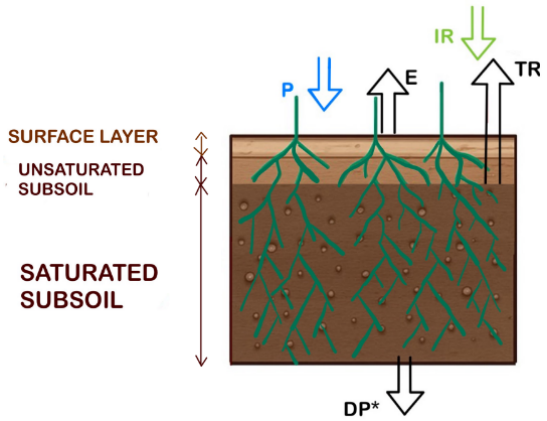

(b)

Figure 4.4: Schematic representation of a volume of soil when no ponding water is present. P indicates precipitation; IR irrigation; E evaporation; TR transpiration; DP percolation losses; WL water level (positive when ponding occurs, negative otherwise).

During the flooded phase, when the field is maintained near **saturation water content**, and the water level is above the surface, the **actual evapotranspiration** (ET_a) can be reasonably approximated by the **crop evapotranspiration** (ET_c).

The **FAO single crop coefficient approach** (Eq. 2.7) was therefore applied for the computation of evapotranspiration. Deep percolation was instead assumed to be constant over the entire study area, with a value of 6 mm/day, as suggested by FAO and by similar studies conducted in nearby regions [41]. This assumption may result in the loss of spatial variability information, since more permeable soil units cannot be distinguished from less permeable ones. However, paddy fields are generally prepared with a compacted and less permeable layer at the bottom to minimize percolation losses, making this approximation acceptable. For this reason field measurement campaigns would be required to accurately quantify saturated hydraulic conductivity values to improve the deep percolation estimation.

As long as the water level remains above the soil surface, the soil moisture content stays close to saturation since the logic of a *water bucket model* ensures that the losses in the subsoil would be always replaced by a water flux from surface to soil. Under these conditions, it make sense that water losses due to evapotranspiration and percolation are directly subtracted from the ponded water layer. The daily water level (WL_i) is updated as:

$$WL_i = WL_{i-1} + P_i - ET_{a,i} - DP_i \tag{4.2}$$

where:

- WL_i and WL_{i-1} are the ponded water levels [mm] at the end of day i and the previous day, respectively;
- P_i is the daily precipitation [mm];
- $ET_{a,i}$ is the actual evapotranspiration [mm day^{-1}];
- DP_i is the deep percolation [mm].

During drying periods, required at specific times of each irrigation strategies because of agronomic practices, the water level falls below the soil surface and the soil moisture decreases and deviates from saturation conditions. In this context, evapotranspiration estimation becomes more complex. The model employs a **dual crop coefficient approach** (Eq. 2.8), in which the soil is divided into two distinct layers:

- a **topsoil layer** (10 cm), responsible for the evaporation component of evapotranspiration, represented by the coefficient K_e;
- a **subsoil layer**, increasing in thickness from 5 cm to 40 cm during the season, contributing to transpiration, represented by the **basal crop coefficient** K_{cb}.

Water stress in both the top and subsoil layers is introduced through two additional coefficients, k_r and k_s, calculated according to the FAO methodology. These coefficients are computed daily as a function of the water deficit in each soil layer, that is the difference between the **saturation water content** and the **actual soil water content** of that layer, using the following equations:

Evaporation reduction coefficient (topsoil). Let $D_{e,i}$ be the depletion of the evaporating layer (topsoil) at day i [mm]. The evaporation reduction coefficient $k_{r,i}$ is defined as:

$$k_{r,i} = \begin{cases} 1, & 0 \le D_{e,i} \le \mathrm{REW}, \\ \dfrac{\mathrm{SAT}_{top} - D_{e,i}}{\mathrm{SAT}_{top} - \mathrm{REW}}, & \mathrm{REW} < D_{e,i} < \mathrm{SAT}_{top}, \\ 0, & D_{e,i} \ge \mathrm{SAT}_{top}, \end{cases} \tag{4.3}$$

where $k_{r,i} \in [0,1]$.

Soil evaporation coefficient. Given the basal crop coefficient $K_{cb,i}$, the maximum crop coefficient $K_{c,\max}$, and the green canopy cover fraction $f_{c,i}$, the soil evaporation coefficient is calculated as:

$$K_{e,i} = \min\Big[k_{r,i}\,(K_{c,\max} - K_{cb,i}),\ (1 - f_{c,i})\,K_{c,\max}\Big], \tag{4.4}$$

with $K_{e,i} \in [0, K_{c,\max}]$.

Transpiration reduction coefficient (Subsoil). Let $D_{r,i}$ be the root-zone water deficit at day i [mm]. The transpiration reduction coefficient is:

$$k_{s,i} = \max\left(0, \min\left[1, \frac{\mathrm{SAT}_{sub} - D_{r,i}}{\mathrm{SAT}_{sub} - \mathrm{RAW}_{sat}}\right]\right), \tag{4.5}$$

ensuring $k_{s,i} \in [0,1]$.

Soil water storage parameters. The main soil hydraulic parameters used in the computation of k_r and k_s are defined as follows.

$$\mathrm{SAT}_{sub} = 1000\,(\theta_{sat,sub} - \theta_{wp,sub})\,Z_r \quad [\mathrm{mm}], \tag{4.6}$$

$$\mathrm{RAW} = p\,\mathrm{TAW}, \qquad \mathrm{RAW}_{sat} = p\,\mathrm{SAT}_{sub}, \qquad p = 0.2, \tag{4.7}$$

$$\mathrm{SAT}_{top} = 1000\,(\theta_{sat,top} - 0.5\,\theta_{wp,top})\,z_e \quad [\mathrm{mm}], \tag{4.8}$$

where: RAW is the *Readily Available Water* (fraction p of TAW), SAT_{sub} is the total storage from wilting to saturation in the subsoil transpiring layer and SAT_{top} is the water storage from wilting to saturation for the same layer.

Readily Evaporable Water (REW). The *Readily Evaporable Water* (REW) depends on soil texture, estimated empirically as:

$$\mathrm{REW} = \begin{cases} 20 - 0.15\,S, & \text{if } S \ge 80, \\ 11 - 0.06\,C, & \text{if } C \ge 50, \\ 8 + 0.08\,C, & \text{otherwise}, \end{cases} \qquad [\mathrm{mm}], \tag{4.9}$$

where S and C are the sand and clay contents (%) of the soil.
Then it is also convenient to define:

$$\text{TAW} = 1000\,(\theta_{fc,sub} - \theta_{wp,sub})\,Z_r \quad [\text{mm}], \tag{4.10}$$

$$\text{TEW} = 1000\,(\theta_{fc,top} - 0.5\,\theta_{wp,top})\,z_e \quad [\text{mm}], \tag{4.11}$$

$$\tag{4.12}$$

Where: TAW is the *Total Available Water* in the root zone, and TEW is the *Total Evaporable Water* in the topsoil layer, and

At this stage, the **actual evapotranspiration** (ET_a) can be computed as:

$$ET_a = ET_0 \times (K_{cb} \cdot k_s + K_e) \tag{4.13}$$

In this case, percolation also becomes a function of the water stress level and the actual water availability. Consequently, percolation reaches its maximum value of 6 mm/day as long as the subsoil moisture remains above the field capacity, and it drops to zero once the subsoil moisture falls below the field capacity.

The daily variation in soil moisture is then updated through a water balance equation, where the soil moisture (SM) at day i depends on the soil moisture of the previous day $(i-1)$ and the daily change in soil water storage (ΔS_i):

$$SM_i = SM_{i-1} + \Delta S_i \tag{4.14}$$

The daily change in soil water storage (ΔS_i) is defined as the difference between incoming and outgoing water fluxes:

$$\Delta S_i = P_i + I_i - ET_{a,i} - DP_i \tag{4.15}$$

where:

- P_i is the daily precipitation [mm];
- I_i is the irrigation applied during day i [mm];
- $ET_{a,i}$ is the actual evapotranspiration [mm day^{-1}];
- DP_i is the deep percolation [mm].

Positive values of ΔS_i indicate an increase in soil water content, while negative values correspond to soil drying.

At this point the water level the **water level** (WL_i) can be computed. It is calculated as a function of the daily soil moisture, assuming that the water table follows the saturation level of the soil. The model computes the vertical position of the water level based on the soil moisture (ϑ) in both the topsoil and subsoil layers, distinguishing the different hydrological conditions depending on whether the water level lies within the topsoil, subsoil, or above the surface (ponded water).

The general formulation for estimating the water level position x_i (below the soil surface) as a function of soil moisture is:

$$x_i = \frac{SM_i - (Z_i \cdot \vartheta_{fc})}{\vartheta_{sat} - \vartheta_{fc}} \tag{4.16}$$

where:

- x_i [m] is the depth of the water level below the soil surface at day i;
- SM_i [mm] is the total soil moisture storage;
- Z_i [m] is the thickness of the soil layer considered;
- ϑ_{fc} [m^3/m^3] is the soil volumetric water content at field capacity;
- ϑ_{sat} [m^3/m^3] is the soil volumetric water content at saturation.

This relation allows identifying the depth at which the soil water content equals the saturation threshold, thus determining the position of the water level.

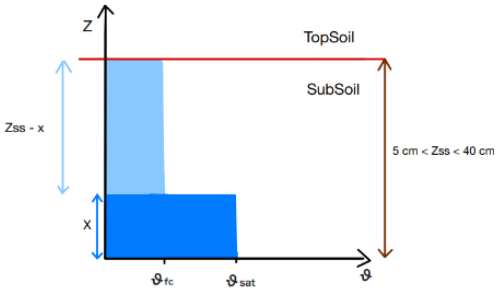

Figure 4.5: Schematic representation of the relationship between subsoil moisture and water level (WL).

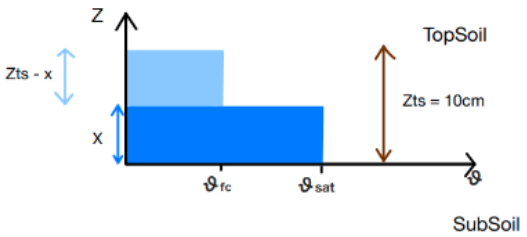

Figure 4.6: Schematic representation of the relationship between surface soil moisture and water level (WL).

Then the model run all these calculation over a grid based on input date above the studied area.

By incorporating the appropriate **irrigation management strategies and scheduling methods**, the model computes the irrigation water requirements in terms of water depth [mm] for each cell of the grid. The **total irrigation volume** required for the study area is then obtained by integrating the water requirement (expressed as water depth) over the cultivated rice areas described in Chapter 3. Each field parcel is assigned its corresponding irrigation depth value. Consequently, the final irrigation volume is computed as the sum of the products between each parcel area and its respective irrigation depth, as follows:

$$V_{\text{irr}} = \sum_{i=1}^{n} A_i \cdot I_i \tag{4.17}$$

where A_i is the area of the i-th field parcel [m^2], and I_i is the corresponding irrigation depth [m].

The rice areas considered for the calculation were derived from the Geoportale Piemonte dataset. Actual rice-cropped areas were available only for 2021 and 2022, and these were directly used for those years. For the remaining years (2018–2020), since no data were available, the rice-cropped area corresponding to 2022 was used instead. This value represents an intermediate condition between 2021 and 2023 and can therefore be considered a reasonable approximation of the average cultivated surface over the study period (about 60,000 ha).

4.3 Irrigation Scenario

Three irrigation strategies were implemented : the traditional **Continuous Flooding** (CF) with wet seeding, **the dry-seeding solution** (DFL) and the more innovative **Alternate Wetting and Drying** (AWD). The implementation of these scenarios draws on evidence from a study conducted in a nearby area [23], which reflects irrigation practices adopted by farmers in Northern Italy, on the technical guidelines provided by the Italian Rice Board (*Ente Nazionale Risi*, ENR) [42] and by the informations shared by AIOS (*Associazione D'Irrigazione Ovest Sesia*). The results are therefore calculated under the hypothesis that all the area is managed with one of the selected irrigation strategy. The exactly irrigation volume can be estimated by considering the proper share of each specific management type that was not available for this study.

Continuous Flooding (CF). On average across the district, fields are maintained with a ponded water layer of about **12 cm (120 mm)** from approximately five days before seeding until ripening, interrupted only by a few short drying periods required for emergence and specific agronomic operations. A first drying period occurs about 15 days after sowing and lasts for around a week. This dry phase is called *the rooting dry period* and is intended to promote the root development of the young plants. Then the field is reflooded until mid late/june when a second herbicide treatment is done. Then the filed

is flooded again until the end of august , coinciding with the final ripening phase, when the field is dried before harvesting, which takes place about one month later. The general scheme consists therefore in three flooding and two drying events. In the model, the five-day pre-sowing flood is accounted for by adding an initial water term to the seasonal irrigation total equal to:

$$W = 120 \text{ mm} + \text{SAT\_TOP} + \text{SAT\_SUB} \tag{4.18}$$

which represents the ponded layer plus the water required to bring the topsoil and subsoil compartments to saturation at the start of the season.

Drying seeding and Delayed flooding (DFL). Unlike the traditional CF, with the DFL the sowing occurs on dry soils, corresponding to no flooded condition. About 35 days after sowing, the first dry herbicide treatment is carried out. However, since herbicide application must be done on wet soil, a first water input occurs. After 48–72 hours, the paddy field is flooded to form a water layer of about 12 cm. Around 15 days later, the first fertilization takes place under flooded conditions, so the outlets remain closed. About 20 days after the first fertilization, the field is drained to allow for a second dry herbicide treatment. After another 48–72 hours, the paddy field is reflooded, restoring the initial water depth. Subsequently, the second and third fertilizations are performed under flooded conditions, and about 45 days after the second herbicide treatment, coinciding with the final ripening phase, the field is dried before harvesting, which takes place about one month later.

Alternate Wetting and Drying (AWD). AWD follows CF during the early stage (wet seeding). Intermittent flooding begins from the tillering stage, and irrigation is applied only when the soil reaches a **critical moisture threshold** (defined by the specific AWD variant), restoring a target ponding depth of 12 cm after each event. According to ENR's recommendations, the operational schedule is as follows:

- **Tillering:** adopt *AWD-strong*, maintaining standing water for 7–10 days after each top-dressing fertilization.
- **Stem elongation:** switch to *AWD-safe* to reduce the risk of rice blast infection.
- **Mid-elongation to early booting:** allow a stronger drying phase to minimize arsenic accumulation in the grain.
- **Booting and flowering:** return to continuous submergence to avoid sterility due to thermal stress.
- **Flowering to milk stage:** maintain continuous flooding to help reduce cadmium content in the grain.
- **Late season (waxy ripening):** resume *AWD-safe*, which is generally beneficial for the final yield.

This management sequence reflects both agronomic constraints (fertilization and disease control) and quality objectives (trace-metal reduction), while maintaining the water-saving potential of AWD compared to the traditional CF regime.

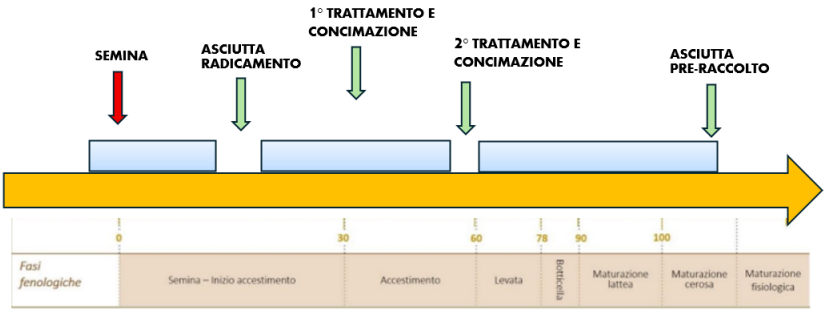

(a) CF

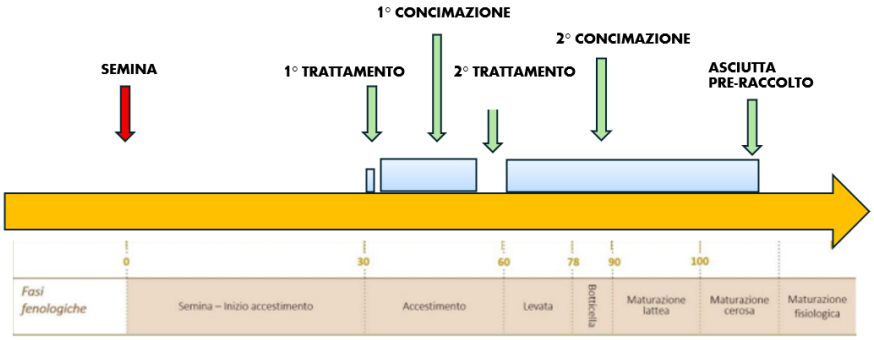

(b) DFL

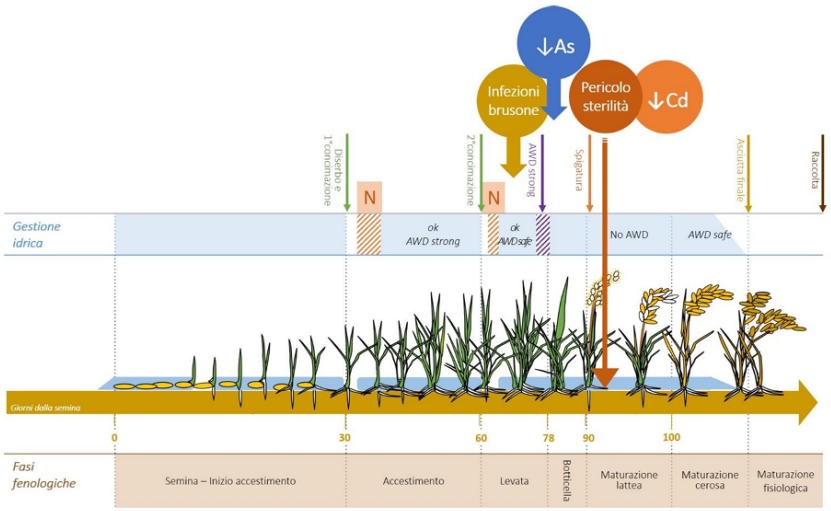

(c) AWD

Figure 4.7: Schematic representation of the three irrigation scenario tested

4.4 Model Implementation

Python environment and libraries

The entire model was implemented in Python 3.12, which served as the primary programming environment for both single point testing and for large-scale simulations. Several open-source libraries were employed to handle numerical computations, data management, and geospatial operations. Table 4.2 provides a summary of the main libraries and their respective roles in the modeling framework.

Table 4.2: Python libraries used in the implementation and their main purposes.

Library	Description and role in the model
`numpy`	Provides fast numerical operations on arrays and matrices [45]. Used to perform vectorized calculations for evapotranspiration, soil moisture, and water balance components.
`pandas`	Used for structured data handling and time-series management [46]. Facilitates the creation of daily dataframes storing simulated variables such as precipitation, irrigation, and evapotranspiration.
`xarray`	Handles multi-dimensional datasets (NetCDF format) containing gridded climate and soil data. Enables efficient reading, slicing, and manipulation of large spatio-temporal datasets [47].
`rasterio`	Manages raster-based geospatial data.[37] Used to export model outputs (e.g., seasonal irrigation requirements) as GeoTIFF maps with georeferencing information compatible with GIS software. The TIFF CRS is EPSG:4326.
`dataclasses`	Defines structured parameter classes (e.g., `RiceParams`) containing crop, soil, and irrigation parameters, simplifying parameter management within 2D the code.
`datetime`	Handles date and time operations, including generation of daily timestamps for the simulation period.
`os`	Used for file and directory management, ensuring automated creation of output folders and file paths.

Qgis-based Environmental data management and tools

Geographical Information System (GIS). A **Geographical Information System (GIS)** is an integrated system of data, hardware, and software designed to acquire, store, manage, analyze, and visualize spatially referenced information. A GIS allows the user to open and create digital maps, produce new geographic information, customize maps for printing or sharing, and perform spatial analyses to support decision-making [48].

Spatial data (or geospatial data) are georeferenced data, meaning that they are associated with specific coordinates within a geographic or projected reference system, which precisely define their position on the Earth's surface.

QGIS was used extensively throughout this work as a key platform for spatial data management and analysis. In particular, it served as an essential interface between the geospatial datasets retrieved from the Piedmont Region Geoportal and the outputs of the irrigation model developed in Python.

The software was first employed to manage and visualize the spatial data related to the *Utilized Agricultural Area* (UAA), downloaded from the regional Geoportal. These datasets were used to identify and classify the cultivated parcels within the boundaries of the irrigation district, distinguishing crop types and quantifying their spatial extent. Using the attribute and field calculator tools, several statistics were derived for each crop category, including the total cultivated surface for each crop, the minimum and maximum crop field extension per each crop type and interannual variations.

Subsequently, QGIS was used to integrate the model outputs, expressed as irrigation water depth (mm) and exported in GeoTIFF format, with the vector layer of rice cultivation parcels. This operation allowed the spatial overlay of irrigation requirements with the actual agricultural parcels, enabling the computation of the total irrigation **volumes** (m^3) by multiplying the modeled irrigation depths by the corresponding cultivated surface areas. This step was essential to translate the model results from depth-based metrics to volumetric quantities directly comparable with operational water management data.

Finally, the QGIS environment was used to produce thematic maps, visualize the spatial variability of irrigation demand across the district, and support the creation of figures included in this thesis. A detailed list of the specific processing and analysis tools used in QGIS is provided below.

Main QGIS tools and operations used:

- Zonal Statistic (overlay of rice parcels and model outputs)
- Field calculator (area computation and volume estimation)
- Statistics by categories (surface analysis by crop type)
- Vector Geoprocessing tools (to cut, clip, extract vectors)
- Reprojection tools (to change outputs CRS from EPSG:4326 to 32632 compatible with Piemonte Region and with meters-based operations for areas and volumes)
- Multilevel B-Spline Interpolation to reduce the spatial resolutions of maps improving the visual quality.
- Vector Analysis to perform some important statistics (e.g. mean, max , min irrigation depth)

4.5 Model testing and consistency check

Before applying the model to the real study area, a series of preliminary tests were performed to verify its internal consistency and hydrological behavior. This step cannot be considered a formal *validation*, as no comparison with observed data was conducted. Rather, it represents a methodological verification aimed at ensuring that the implemented equations correctly reproduce the expected physical response of the system.

The objective of this test phase was to assess the model's ability to simulate the daily evolution of soil moisture (SM) and water level (WL) under different hydrological conditions and irrigation regimes. In particular, three main types of simulations were carried out:

1. **Single water input tests**, used to verify the correct functioning of the *water-bucket filling logic* under controlled conditions. These tests involved the application of isolated precipitation or irrigation events with different magnitudes, starting from distinct initial soil moisture and water level configurations.

2. **Rainfed simulations**, performed using real climatic data (precipitation and evapotranspiration) from contrasting years — specifically 2018 (wet) and 2022 (dry) — to observe how the model reproduces soil drying and moisture replenishment dynamics in the absence of irrigation.

3. **Irrigation scenario simulations**, in which the model was run under the three management practices described (Continuous Flooding, Alternate Wetting and Drying, and Dry Seeding with Delayed Flooding). These tests aimed to check that the implemented irrigation scheduling correctly generated the expected alternation of flooding and drying phases.

The outputs of these tests consist of daily time series of soil moisture and water level, which allow assessing the temporal dynamics and verifying the model's internal consistency before the large-scale spatial application.

4.6 Work Flow

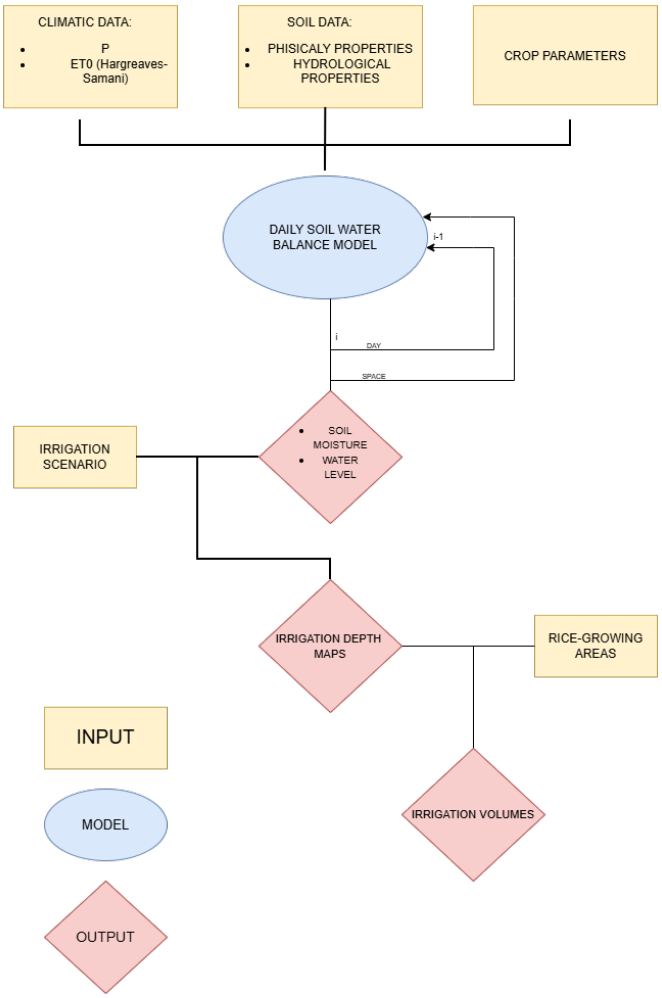

Figure 4.8: Methodological workflow of the Thesis

Chapter 5

Results

This chapter presents and discusses the results obtained from the implementation of the soil water balance model developed for the estimation of irrigation requirements in paddy rice cultivation. The outputs are analysed at both temporal and spatial scales, with the aim of evaluating the model's behaviour, quantifying the irrigation demand associated with different management strategies, and assessing the potential for water saving within the study area. The analysis is structured into several parts. First, Climatic and Soil data analysis and visualizations are presented. Then a preliminary validation is carried out by analysing the simulated daily evolution of soil moisture (SM) and water level (WL) in representative grid cell and in different initial conditions and different water inputs, in order to verify the internal consistency of the model and its response to climatic, irrigation inputs and to losses (ETa, DP). Then the spatial distribution of irrigation requirements in terms of irrigation depth is presented for each irrigation strategy (Continuous Flooding – CF, Alternate Wetting and Drying – AWD, and Dry Seeding with Delayed Flooding – DLF), for the whole Po basin area over the 2018–2022 period and for Associazione d'Irrigazione Ovest Sesia (AIOS), the pilot district of the study, where total irrigation volumes and their interannual variability are analysed for the 2018–2022 period. Finally the spatial variability of results is discussed in order to asses which are the main drivers of irrigation requirements for the area.

5.1 Climatic Data

5.1.1 PO basin

CLIMATIC DATA [mm]	PRP	ET0
2018	455	776
2019	433	788
2020	410	789
2021	230	793
2022	287	856
FIVE YEARS	363	800

Figure 5.1: Table showing climatic data input values over PO basin over the 2018-2022 period.

The data show a temporal deterioration of hydrological conditions both in terms of precipitation (PRP) and reference evapotranspiration (ET0). From 2018 to 2020, the situation appears relatively stable, with average precipitation ranging between 410 and 460 mm and ET0 values around 770–790 mm. Starting from 2021, a marked worsening of hydrological conditions can be observed, with a sharp decrease in rainfall (down to 280 mm in 2022) and an increase in evapotranspiration (up to about 850 mm).

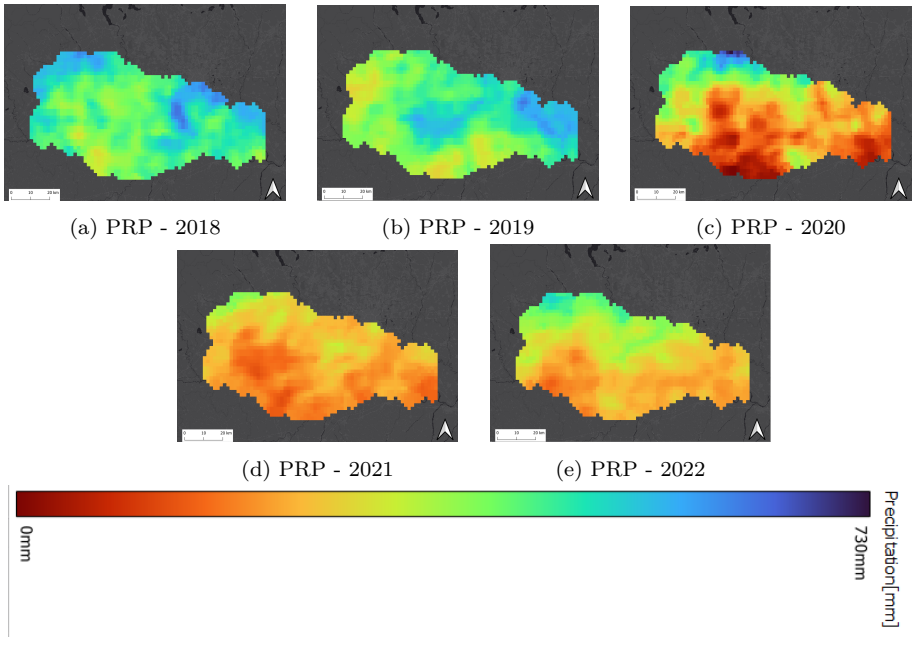

(a) PRP - 2018 (b) PRP - 2019 (c) PRP - 2020

(d) PRP - 2021 (e) PRP - 2022

(f) BAR

Figure 5.2: Total cumulated Precipitation during the rice growing season (25 apr. - 25 Sep.) on the Po Basin for the different analyzed years.

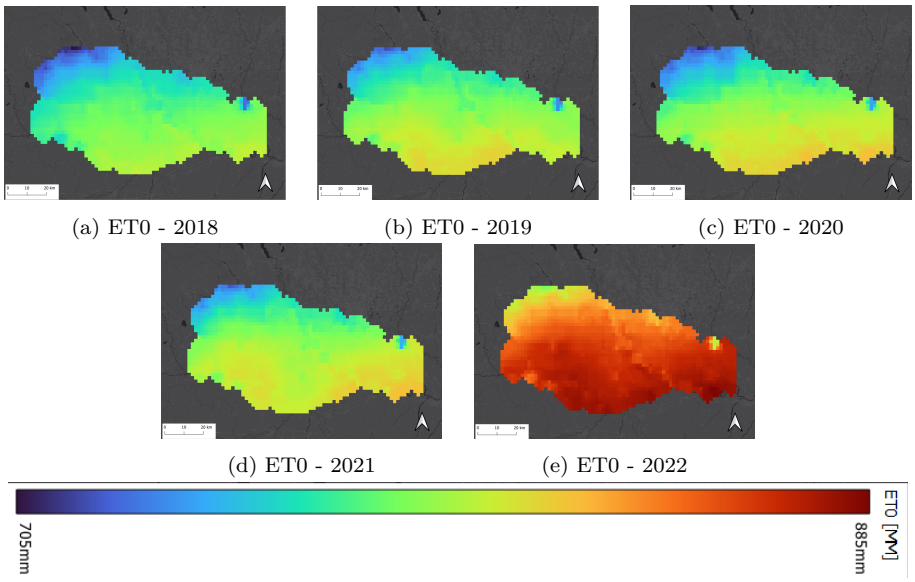

(a) ET0 - 2018 (b) ET0 - 2019 (c) ET0 - 2020

(d) ET0 - 2021 (e) ET0 - 2022

(f) BAR

Figure 5.3: Reference Evapotranspiration cumulated during the rice growing season (25 apr. - 25 Sep.) on the Po Basin for the different analyzed years.

From a spatial variability perspective, the situation appears simpler for reference evapotranspiration, which remains almost identical during the first four years, showing a slight decreasing trend from the southeast toward the northwest. In 2022, the spatial distribution remains similar, but with a clear overall increase in values. The situation is instead more complex in terms of precipitation spatial variability. Conditions remain almost unchanged during the first two years; however, in 2020, despite an average value similar to the previous years, spatial differences become more pronounced, with a noticeable gradient developing from the southeast to the northwest. Such gradients, though less marked, are still present in 2021 and 2022, when the main issue is the significant overall reduction in average precipitation across the entire area. Consequently, as already highlighted, 2022 stands out as the worst year from a climatic point of view. While 2021 also showed severe rainfall deficits, it did not record a corresponding increase in temperatures and consequently in evapotranspiration, which partly balanced the overall impact. In contrast, 2022 experienced a deterioration in both variables simultaneously, leading to an overall fragile climatic condition.

5.1.2 AIOS

CLIMATIC DATA AIOS [mm]	PRP	ET0
2018	425	772
2019	380	788
2020	420	784
2021	205	796
2022	259	858
FIVE YEARS	338	800

Figure 5.4: Table showing climatic data input values for AIOS over the 2018-2022 period.

The climatic data show a clear temporal trend for both precipitation (PRP) and reference evapotranspiration (ET0) over the 2018–2022 period. From 2018 to 2020, conditions appear relatively stable, with average precipitation around 410–420 mm and ET0 values between 770 and 790 mm. Starting from 2021, a significant deterioration of hydrological conditions can be observed: rainfall sharply decreased (down to 259 mm in 2022), while ET0 progressively increased, reaching its maximum in 2022 (858 mm). This combination of lower rainfall and higher evaporative demand marks 2022 as the driest and most critical year in the entire observation period.

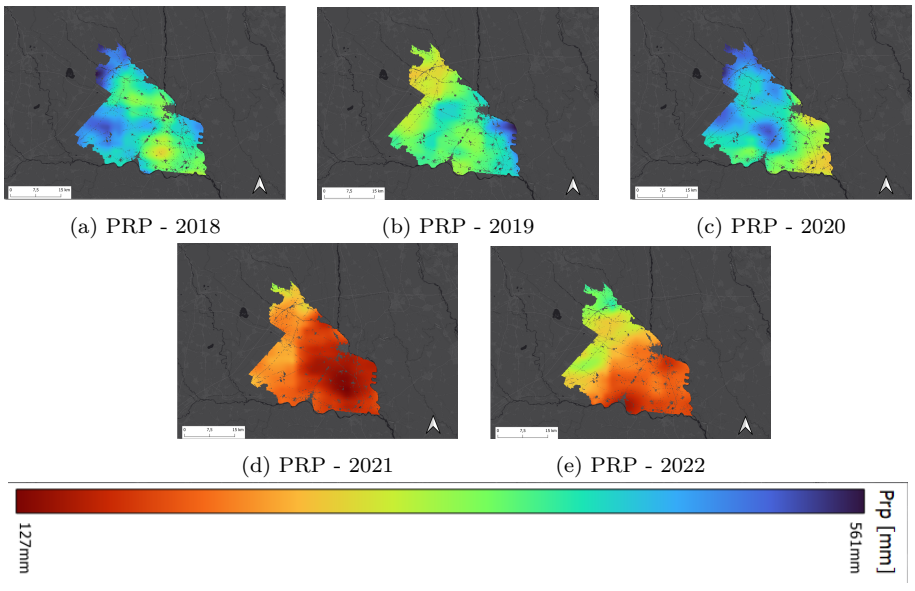

(a) PRP - 2018 (b) PRP - 2019 (c) PRP - 2020

(d) PRP - 2021 (e) PRP - 2022

(f) BAR

Figure 5.5: Total cumulated Precipitation during the rice growing season (25 apr. - 25 Sep.) on the AIOS district for the different analyzed years.

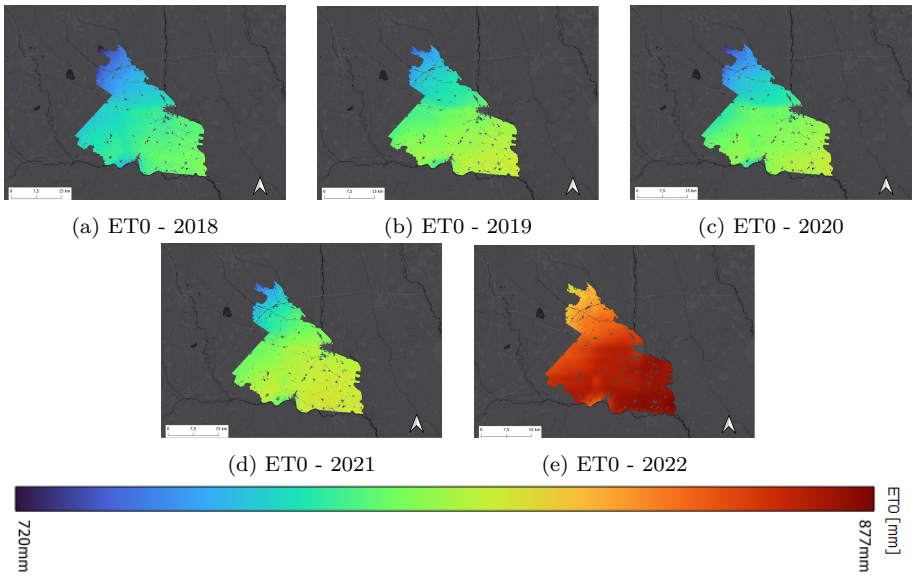

(a) ET0 - 2018 (b) ET0 - 2019 (c) ET0 - 2020

(d) ET0 - 2021 (e) ET0 - 2022

(f) BAR

Figure 5.6: Reference Evapotranspiration cumulated during the rice growing season (25 apr. - 25 Sep.) on the AIOS district for the different analyzed years.

From a spatial perspective, ET0 displays relatively low variability across the study area. During the first four years, values remain almost homogeneous, showing a mild decreasing gradient from southeast to northwest. In 2022, this spatial pattern persists but with a noticeable overall increase in ET0 levels, indicating a generalized rise in atmospheric water demand. The temporal evolution of precipitation (Fig. 5.5) shows a clear interannual variability. During 2018–2019, rainfall was relatively abundant and evenly distributed, with slightly higher values in the northern and central sectors. In 2020, although the average remained similar (420 mm), a more evident southeast–northwest gradient emerged, with drier conditions in the southern part. A significant decline occurred in 2021, when total precipitation dropped to almost half of the 2018–2020 average, particularly affecting the southern and central areas. The trend further worsened in 2022, which recorded the lowest values of the period (259 mm) and a widespread deficit across the entire region, with only marginally wetter conditions in the north.

Overall, the data highlight a progressive reduction in both rainfall amount and spatial uniformity, culminating in 2022 as the driest and most critical year.

5.2 Soil Data

5.2.1 PO basin

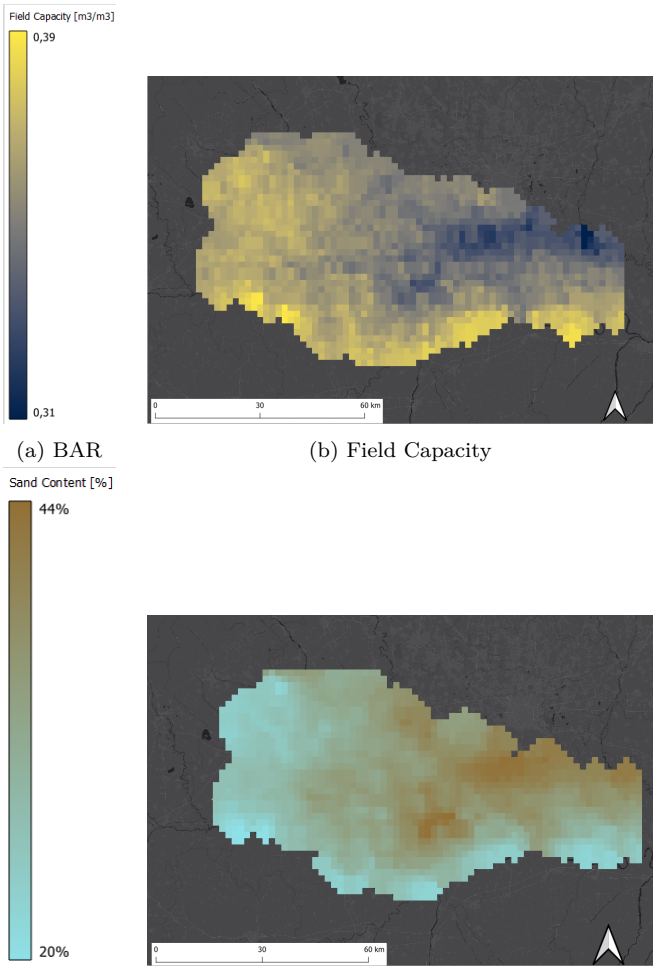

(a) BAR (b) Field Capacity

(c) BAR (d) Sand content

Figure 5.7: Field capacity and sand content over the Po Basin.

Figure 5.7 shows the spatial distribution of field capacity (FC) and sand content over the Po Basin. The map of FC highlights higher values in the central and eastern parts of the study area, and lower values in the western and southern zones. The sand content map displays a complementary pattern: areas with higher sand content correspond to lower field capacity values, confirming the inverse relationship between the two variables. This behaviour is consistent with soil physics: fine-textured soils retain more water due to higher microporosity, whereas sandy soils show lower water retention because of faster drainage.

5.2.2 AIOS

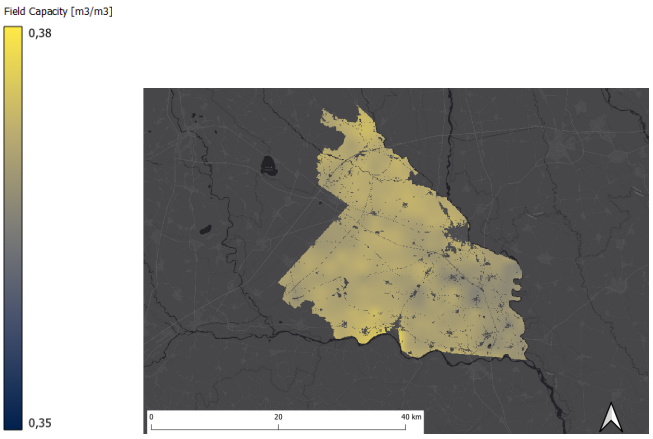

(a) BAR (b) Field Capacity

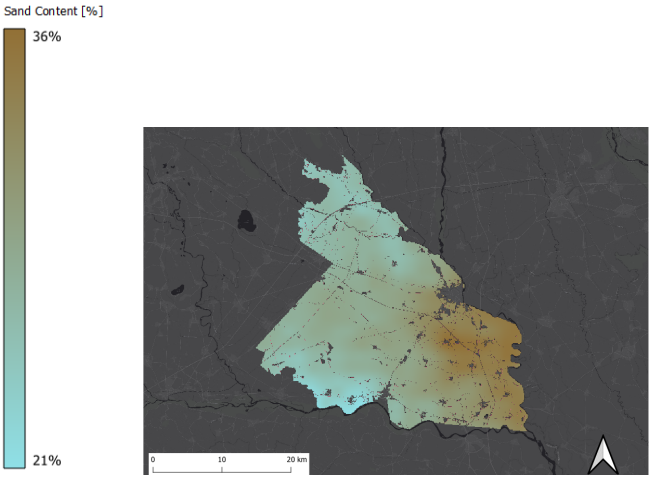

(c) BAR (d) Sand content

Figure 5.8: Field capacity and sand content over AIOS.

Figure 5.9 displays the spatial distribution of field capacity (FC) and sand content within the AIOS area. Compared to the entire Po Basin, the variability of both parameters appears more limited. Field capacity values range within a narrower interval, indicating a relatively homogeneous soil structure. Similarly, sand content shows moderate spatial variability, with slightly higher values concentrated in the southern sector of the area. Overall, the two maps exhibit an opposite spatial pattern, with areas of higher sand content corresponding to slightly lower field capacity values, although the contrast is less pronounced than at the basin scale.

5.3 Model internal consistency results

This section presents the results of the preliminary consistency tests described in Section 4.5. The purpose of these analyses was to verify the internal coherence of the model structure and its ability to reproduce the expected physical behavior of a paddy field system under different hydrological conditions.

5.3.1 Single water input test

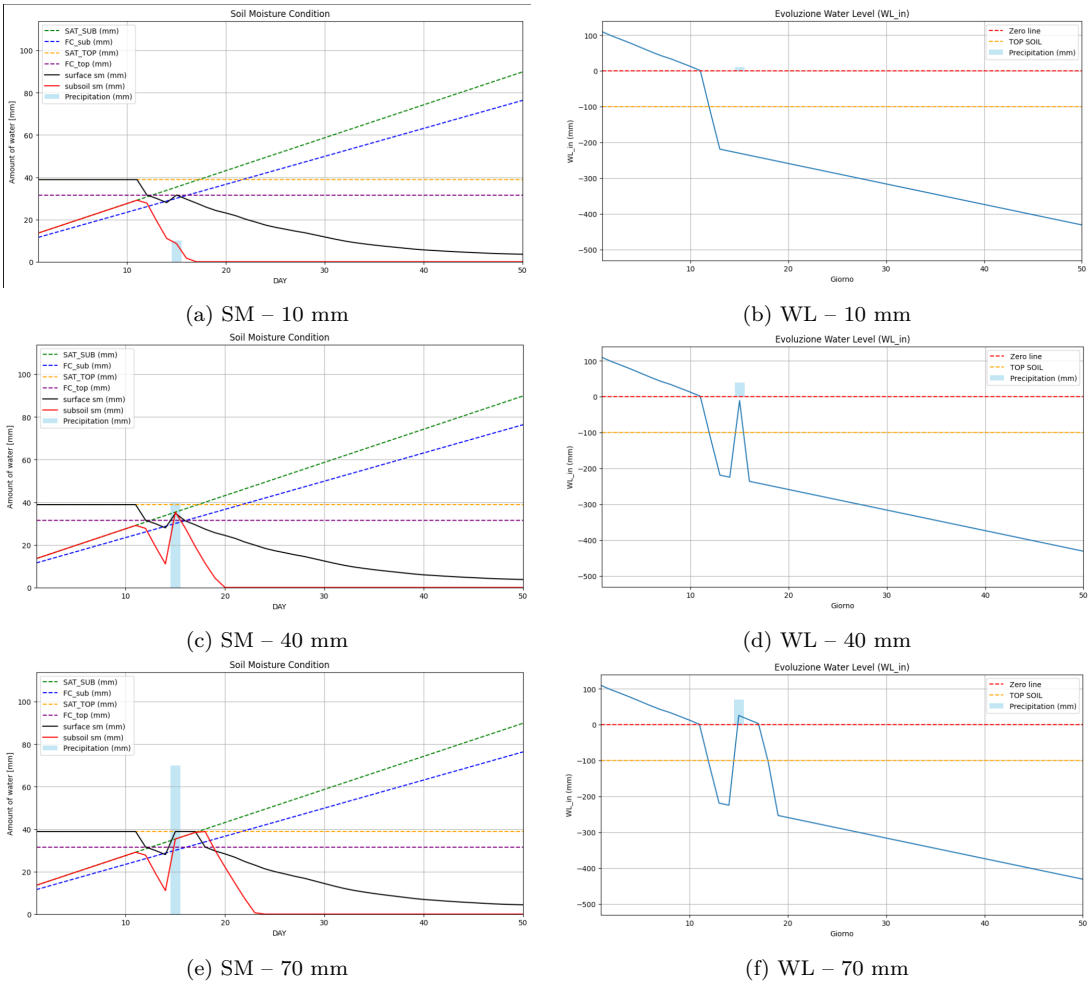

(a) SM – 10 mm

(b) WL – 10 mm

(c) SM – 40 mm

(d) WL – 40 mm

(e) SM – 70 mm

(f) WL – 70 mm

Figure 5.9: Comparison of soil moisture (SM) and water level (WL) evolution for three different water input with a starting WL position in the subsoil.

Several simulations with a single artificial water input were performed to verify the model's response to increasing water amounts starting from different initial conditions of soil saturation. The results (Fig. 5.9) show the expected transition between dry, saturated, and flooded states. When a small water input (10 mm) is applied, the soil moisture in the top layer increases until field capacity is reached, with negligible effect on the subsoil

or water level. For larger inputs (40–70 mm), both layers reach saturation, and the water level progressively rises above the surface, indicating ponding. These results confirm the correct implementation of the water-bucket filling logic and the internal consistency of the model equations.

5.3.2 Real case Rainfed

The model was then run using real climatic data from 2018 and 2022, representing opposite hydrological conditions. Figure 5.10 clearly shows how the model reproduces the effect of precipitation variability on soil water dynamics. In 2018, characterized by frequent and well-distributed rainfall, both topsoil and subsoil moisture increase periodically, while the water level remains below the surface. In contrast, the 2022 season shows limited and irregular rainfall, resulting in progressive soil drying and lower overall moisture levels. These results highlight the model's ability to reflect the influence of climatic variability, confirming that irrigation is essential to sustain rice cultivation under dry-year conditions.

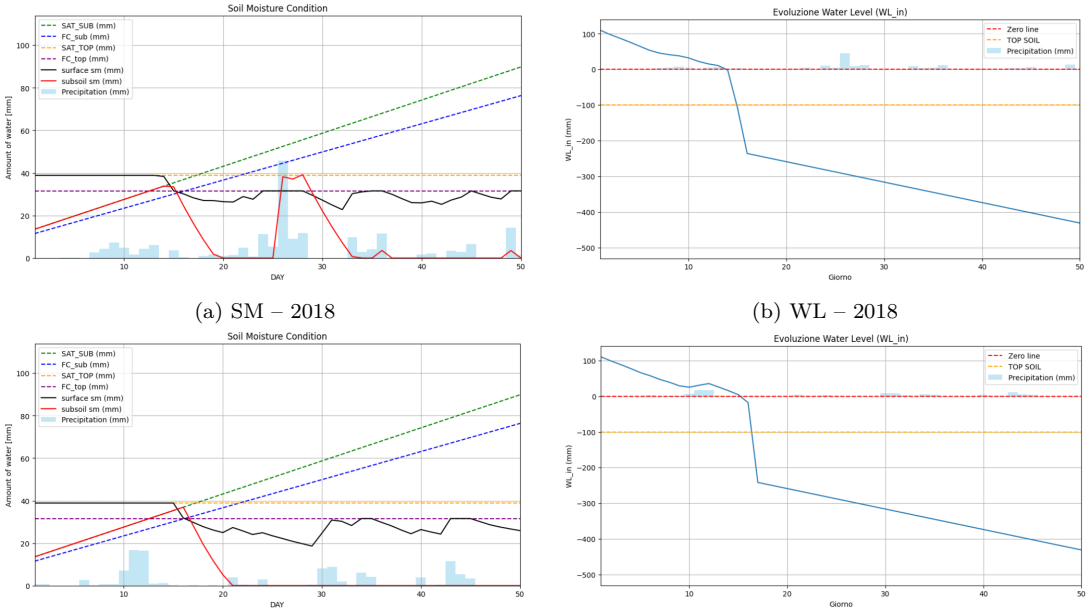

(a) SM – 2018

(b) WL – 2018

(c) SM – 2022

(d) WL – 2022

Figure 5.10: Comparison of soil moisture (SM) and water level (WL) evolution for two different real case. a) and b) refers to climatic data from 2018 while c) d) refers to 2022.

5.3.3 Real case Irrigation

Finally, the model was tested under the three irrigation management strategies described before: Continuous Flooding (CF), Dry Seeding with Delayed Flooding (DFL), and Alternate Wetting and Drying (AWD). The simulated water level dynamics (Fig. 5.11) correctly reflect the characteristic behavior of each irrigation regime. In CF, the water level remains almost constant, with short drying phases for agronomic operations. In DFL, flooding occurs only after about one month from sowing, consistent with the delayed management schedule. In AWD, the alternation between flooding and drying cycles is clearly reproduced, confirming the model's ability to represent variable irrigation timing. These results demonstrate that the model behaves coherently under different irrigation conditions and that its structure correctly translates management practices into hydrological responses.

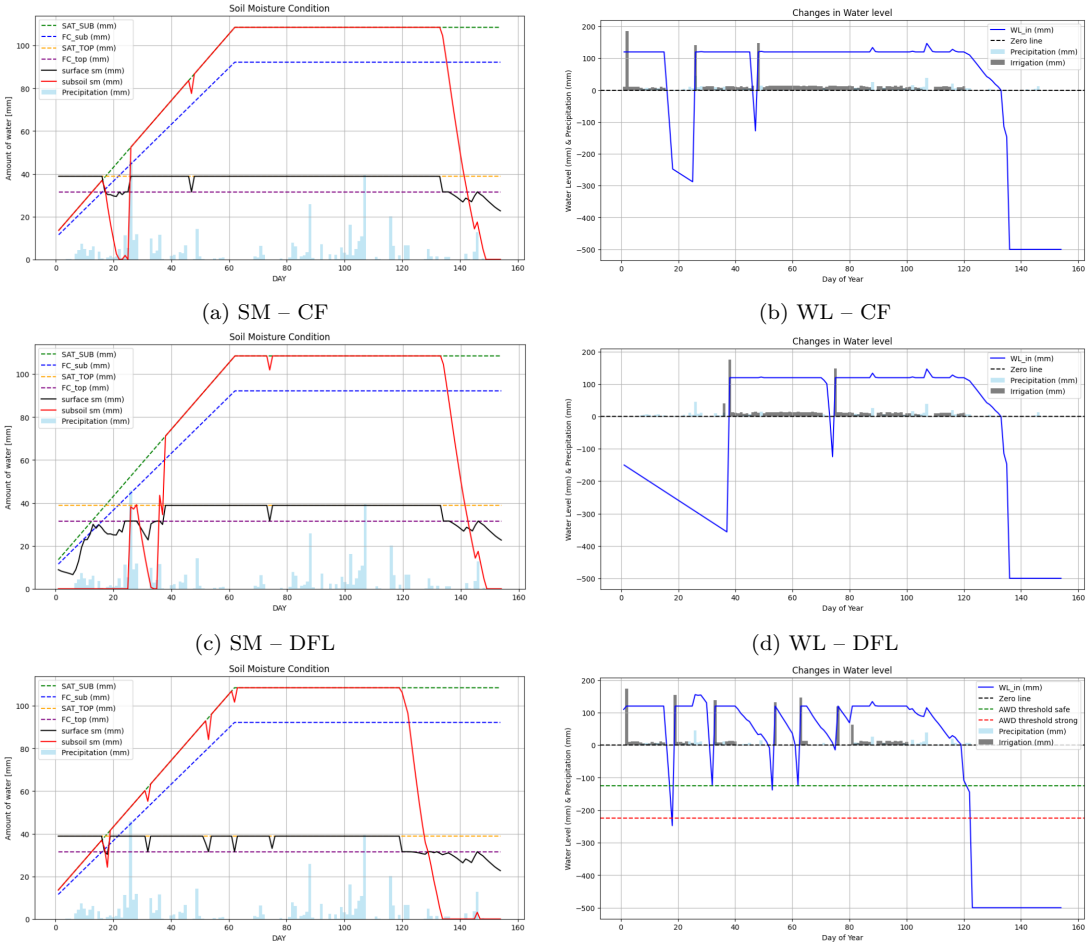

(a) SM – CF

(b) WL – CF

(c) SM – DFL

(d) WL – DFL

(e) SM – AWD

(f) WL – AWD

Figure 5.11: Comparison of soil moisture (SM) and water level (WL) evolution for the three different irrigation strategies.

Overall, the consistency tests confirm that the model is stable, physically coherent, and capable of reproducing the expected dynamics of soil moisture and water level under different climatic and management conditions. These checks represent a necessary methodological step to ensure model reliability before its spatial application over the Po Basin and AIOS district.

5.4 Irrigation depth Results over the PO basin

As already explained in chapter 4, the model produces irrigation depth output maps over a large portion covering the main rice cropped cultivation in Italy. In this section the results for this 2.2km grids are presented for the three irrigation strategies over the analyzed period.

The results are summarized in the table below :

IRRIGATION DEPTH [mm]	CF	DFL	AWD
2018	1542	1107	1456
2019	1583	1197	1473
2020	1555	1151	1499
2021	1718	1286	1606
2022	1796	1365	1638
FIVE YEARS	1639	1221	1534
DIFF-CF	0	-25%	-7%

Figure 5.12: Statistic of Irrigation depth over the main Italian rice cropped area

On average, the Continuous Flooding (CF) method required the largest amount of irrigation water, with a mean value of approximately 1639 mm per season. This result is coherent with the traditional practice of maintaining a constant water layer throughout the growing cycle, which leads to higher water consumption.

The Dry Seeding with Delayed Flooding (DFL) scenario consistently shows the lowest irrigation depth, with an average reduction of about 25–30% compared to CF. This reduction is mainly due to the absence of flooding during the early stages of the crop cycle and the shorter overall duration of inundation.

The Alternate Wetting and Drying (AWD) strategy represents an intermediate condition, requiring on average 1534 mm, which is about 6–7% lower than CF but slightly higher than DFL. The alternation of drying and reflooding periods allows for substantial water savings.

The interannual variability observed in the table mirrors climatic fluctuations across the five years. The lowest irrigation requirements were recorded in 2018–2020, corresponding to relatively wetter conditions, while 2021 and 2022 show a marked increase, with 2022—identified as the second driest year since 1958—reaching the highest simulated irrigation depths under all scenarios.

The maps also allow to observe the spatial variability of the irrigation depth requirements over the area.

5.4.1 Continous Flooding (CF)

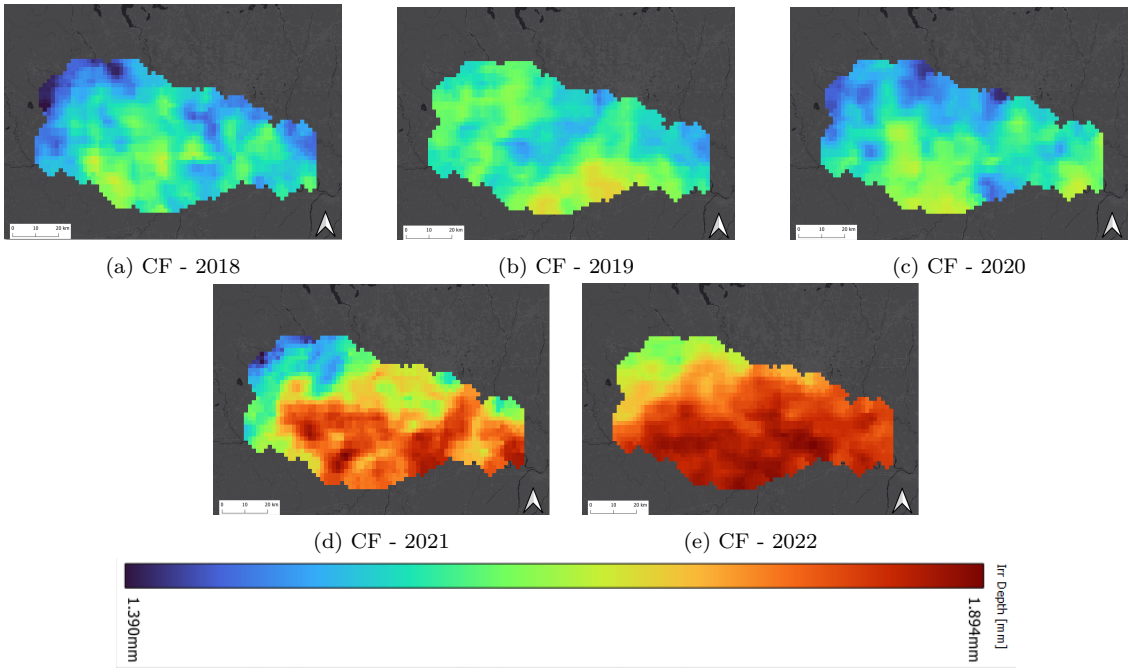

(a) CF - 2018 (b) CF - 2019 (c) CF - 2020

(d) CF - 2021 (e) CF - 2022

(f) BAR

Figure 5.13: Irrigation depth over the studied area over 2018-2022 period with the continous flooding irrigation strategy.

The maps above show the irrigation water depth across the entire study area for the five years under analysis fo the CF strategy. From the maps, it can be clearly observed that the situation remained almost stable during the first three years, with values ranging between 1400 and 1500 mm. The situation drastically worsened starting from 2021, reaching its peak in 2022, when almost the whole area recorded the highest estimated values of around 1800 mm. The year 2021 presents a peculiar situation, with values ranging from near the minimum estimated 1380 mm in the north-western zone to almost 1900 mm in the southern zone, showing a gradient of about 500 mm.

5.4.2 Dry seeding and delayed flooding (DFL)

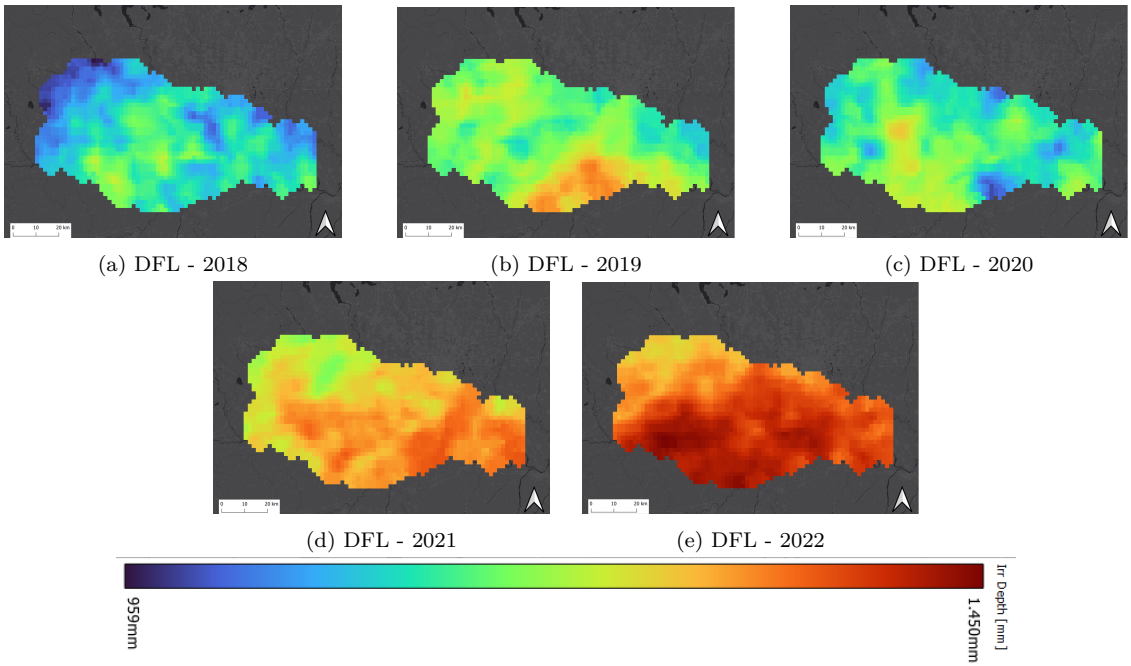

(a) DFL - 2018 (b) DFL - 2019 (c) DFL - 2020

(d) DFL - 2021 (e) DFL - 2022

(f) BAR

Figure 5.14: Irrigation depth over the studied area over 2018-2022 period with the Dry seeding and delayed flooding irrigation strategy.

The results obtained for the DFL strategy are almost identical to those obtained for CF in terms of spatial variability. The difference lies in the fact that here the values range from a minimum of 959 mm to a maximum of 1450 mm. This can be explained by the fact that DFL is managed like CF but with a one-month delay in flooding.

5.4.3 Alternate wetting drying (AWD)

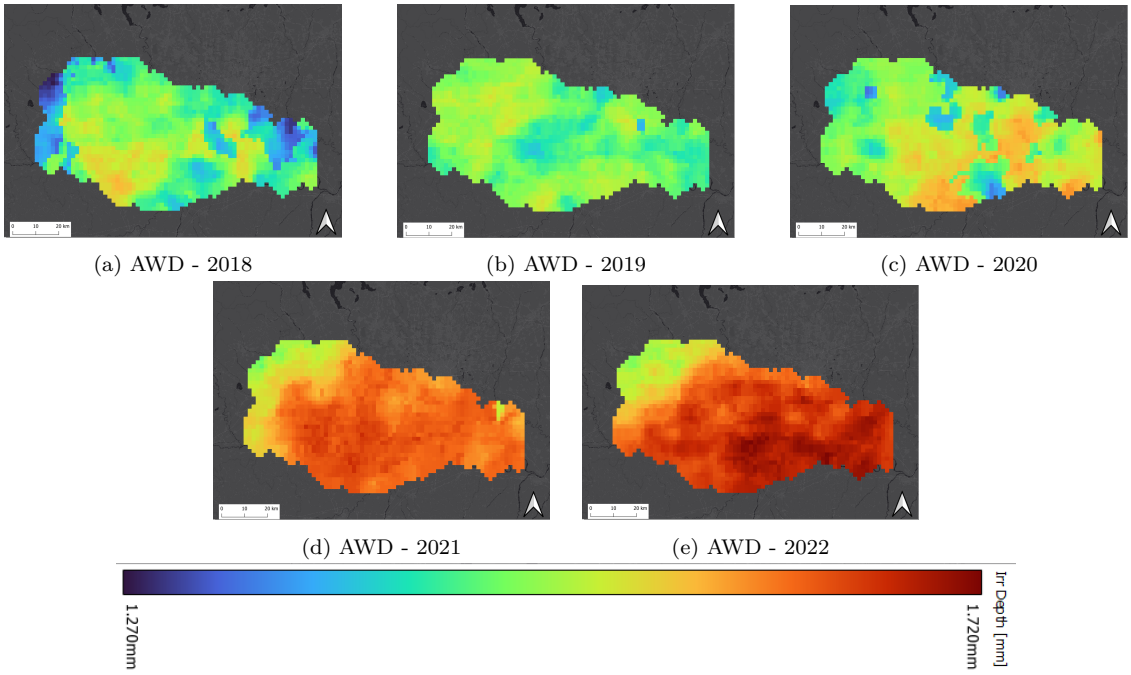

(a) AWD - 2018 (b) AWD - 2019 (c) AWD - 2020

(d) AWD - 2021 (e) AWD - 2022

(f) BAR

Figure 5.15: Irrigation depth over the studied area over 2018-2022 period with the Dry seeding and delayed flooding irrigation strategy.

The results obtained for the AWD strategy are also, in this case, similar to the previous ones in terms of spatial variability. The main difference lies in the fact that for the first three years the results appear less smooth. In fact, there are "patchy" areas with lower peaks surrounded by higher values. This could be due to the fact that this type of irrigation is based on alternating wetting and drying cycles triggered by threshold values that, once reached, activate irrigation events. Consequently, even small localized rainfall events can extend the drying phases, resulting in a lower number of irrigation events. This strategy can be considere more sensitive to rainfall events compared to the others. In this case, the values range from a minimum of 1270 mm to a maximum of 1720 mm.

5.4.4 Mean Comparison

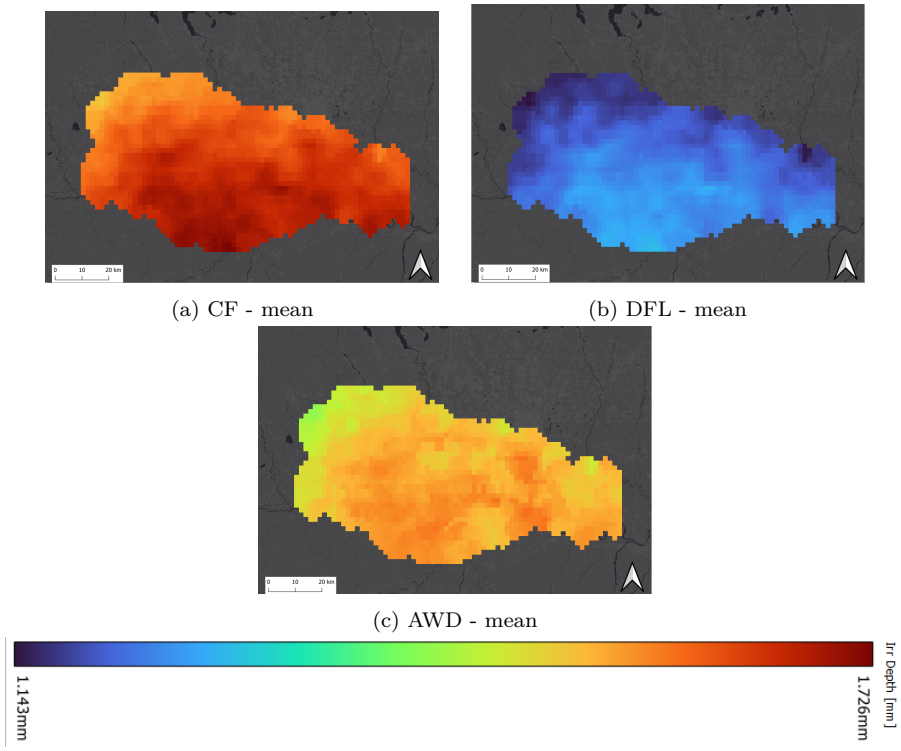

(a) CF - mean

(b) DFL - mean

(c) AWD - mean

(d) BAR

Figure 5.16: Comparison between the three irrigation strategies results averaged over the 5 years period considered .

The maps above compare the average values over the five years for the three strategies. The value scale is the same for all three, allowing for immediate comparison, and ranges from a minimum of 1143 mm estimated in the north-western part of the area for the DFL strategy to a maximum of 1726 mm for the CF strategy in the southern zone. The results clearly show that, in terms of average irrigation depth, CF is the most water-consuming strategy, AWD represents an intermediate solution, and DFL the least demanding. Moreover, it can be observed that for all three strategies there is a consistent pattern, with higher values concentrated in the southern area and lower ones in the north-western zones.

5.5 AIOS results

Located along the western edge of the main rice-growing district, AIOS corresponds to the areas where the lowest irrigation values were identified in the previous spatial analyses. As a result, the average results obtained for this zone are perfectly consistent with those of the entire study area, effectively representing a smaller-scale replica of the overall hydrological behavior even from a spatial distribution point of view.

5.5.1 Irrigation Depth

The results obtained for the AIOS area show an increasing trend in average irrigation depth for all three strategies over the 2018–2022 period. During the first three years (2018–2020), differences among strategies remain limited, while from 2021 onward a marked increase can be observed for all, with a peak in 2022.

In absolute terms, Continuous Flooding (CF) is the most water-consuming strategy, with a five-year average of about 1650 mm, followed by Alternate Wetting and Drying (AWD) with 1538 mm, whereas Delayed Flooding (DFL) proves to be the water saving solution averaging 1233 mm. The differences between the strategies remain relatively stable over time: DFL allows an average water saving of about 25% compared to CF, while AWD represents an intermediate solution, reducing irrigation depth by around 7%. When comparing the first and last years of the analysis (2018 vs. 2022), it can be observed that DFL shows the largest increase in irrigation depth, followed by CF, while AWD exhibits the smallest variation. This indicates that **AWD is less sensitive to interannual climatic variability, making it a promising and more resilient irrigation strategy in the context of climate change adaptation**.

IRRIGATION DEPTH [mm]	CF	DFL	AWD
2018	1560	1122	1487
2019	1585	1188	1485
2020	1563	1166	1478
2021	1732	1290	1610
2022	1819	1400	1631
FIVE YEARS	1652	1233	1538
DIFF-CF	0	25	7

(a) CF - mean

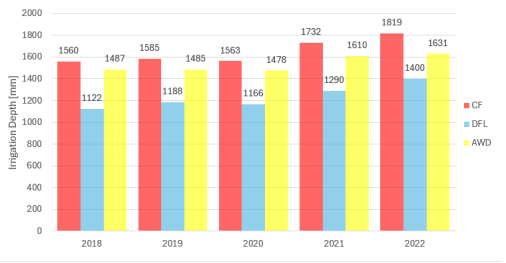

(b) DFL - mean

Figure 5.17: Statistic of Irrigation depth over AIOS for the three different irrigation strategies.

5.5.2 Continuous flooding (CF)

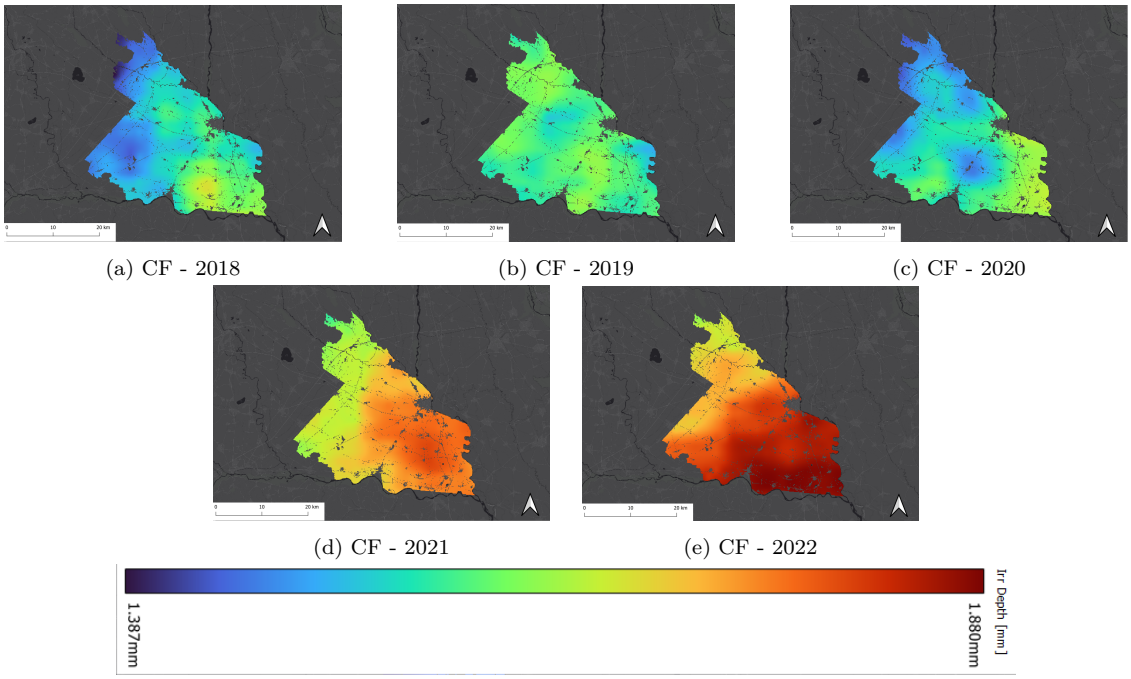

(a) CF - 2018 (b) CF - 2019 (c) CF - 2020

(d) CF - 2021 (e) CF - 2022

(f) BAR

Figure 5.18: Irrigation depth in AIOS district over 2018-2022 period with the continuous flooding irrigation strategy.

The maps above show the irrigation water depth over the AIOS district for the 2018–2022 period under the Continuous Flooding (CF) strategy. It can be observed that the situation remained relatively stable during the first three years, with values mostly ranging between 1400 and 1500 mm. Starting from 2021, irrigation demand significantly increased, with higher values concentrated in the southern part of the district and slightly lower ones toward the northwest.

The 2022 season represents the most critical year, showing a widespread increase in irrigation depth, with almost the entire area reaching values close to 1800 mm. The presence of such high and spatially uniform values reflects the severe climatic conditions of that year, already highlighted in the climatic data analysis.

5.5.3 Dry seeding and delayed flooding (DFL)

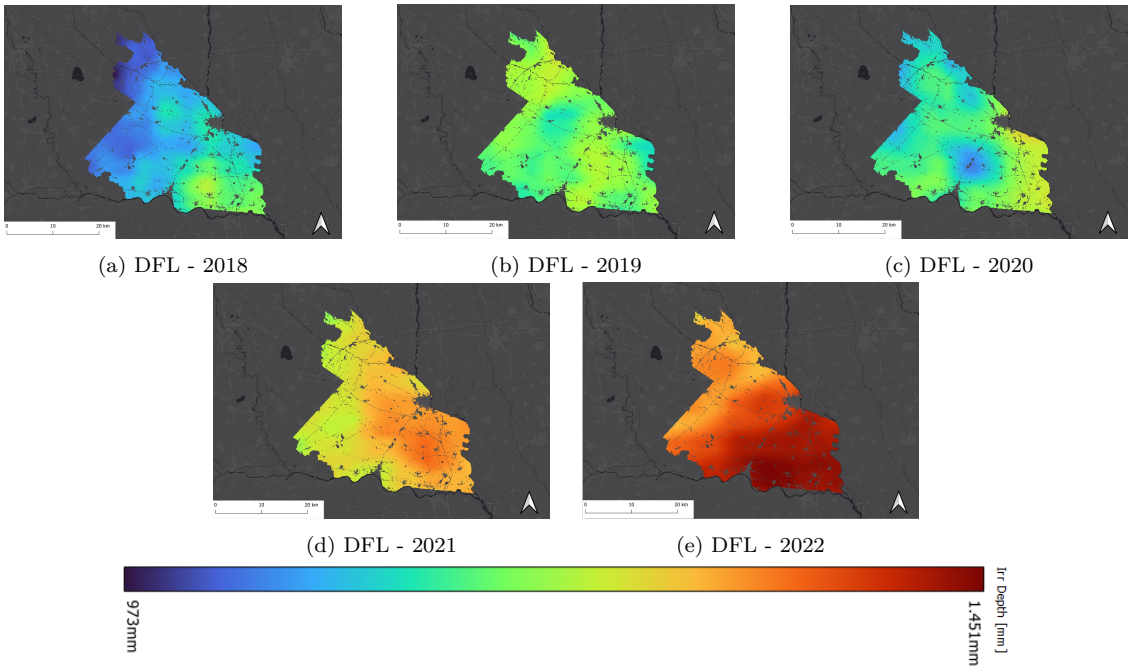

(a) DFL - 2018 (b) DFL - 2019 (c) DFL - 2020

(d) DFL - 2021 (e) DFL - 2022

(f) BAR

Figure 5.19: Irrigation depth in AIOS district over 2018-2022 period with the Dry seeding and delayed flooding (DFL) irrigation strategy.

The irrigation depth results for the DFL strategy in the AIOS district show a trend consistent with that observed for the entire study area. During the first three years (2018–2020), values remain fairly stable, ranging between 950 and 1200 mm, while a noticeable increase occurs from 2021, reaching the highest levels in 2022, when most of the district records values around 1400–1450 mm.

As it was for the entire rice area, the spatial distribution closely resembles that of the CF strategy but the overall irrigation depths are considerably lower. This difference is mainly due to the delayed flooding management, which postpones the initial submersion phase by about one month, thereby reducing the total irrigation demand.

5.5.4 Alternate wetting drying (AWD)

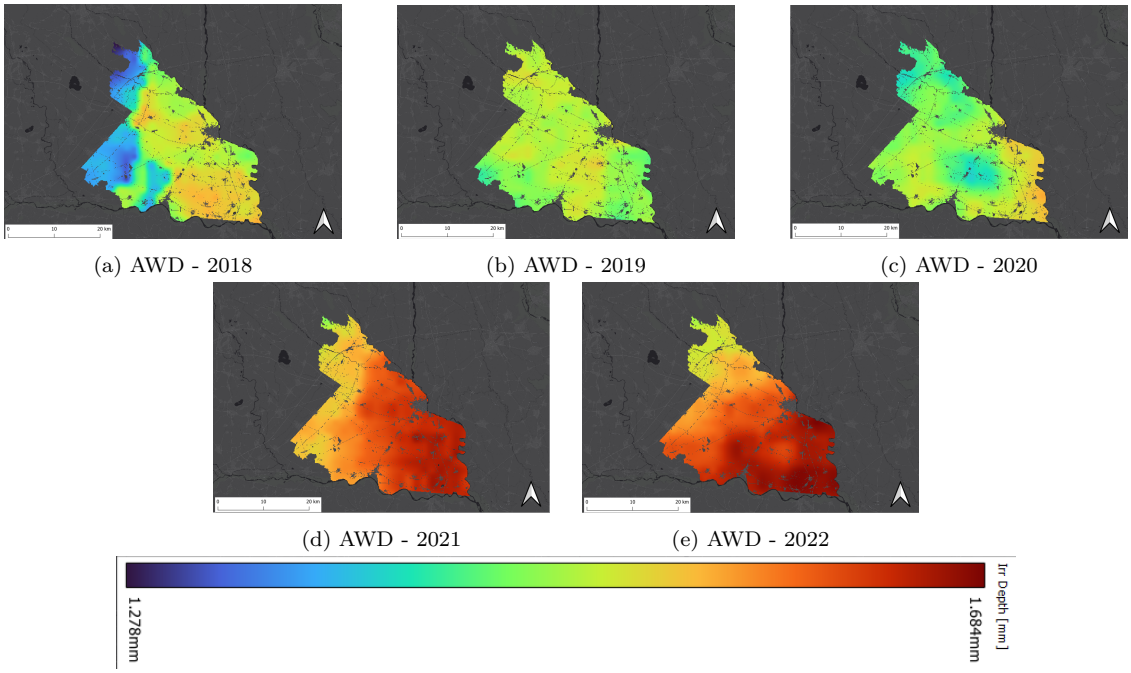

(a) AWD - 2018 (b) AWD - 2019 (c) AWD - 2020

(d) AWD - 2021 (e) AWD - 2022

(f) BAR

Figure 5.20: Irrigation depth in AIOS district over 2018-2022 period with the Alternate wetting and drying irrigation strategy.

The results obtained for the AWD strategy in the AIOS district confirm the trend already observed for the entire study area. Irrigation depths remain relatively stable during the first three years (2018–2020), with values ranging between 1200 and 1500 mm, and then increase significantly in 2021 and 2022, reaching maximum values close to 1650–1700 mm in the southern part of the district.

The spatial distribution is consistent with the other irrigation strategies, showing slightly lower values in the north-western zone and higher ones toward the south. The alternating wetting and drying cycles make the strategy more sensitive to local rainfall variability, which can explain some patchy patterns visible in the earlier years. AWD represents an intermediate condition between CF and DFL in terms of water demand.

5.5.5 Irrigation Volume

IRRIGATION VOLUME [Mm3]	CF	DFL	AWD
2018 *	928	664	887
2019 *	956	717	899
2020 *	933	698	889
2021	1053	787	980
2022	1079	828	971
FIVE YEARS	990	739	923

(a) CF - mean

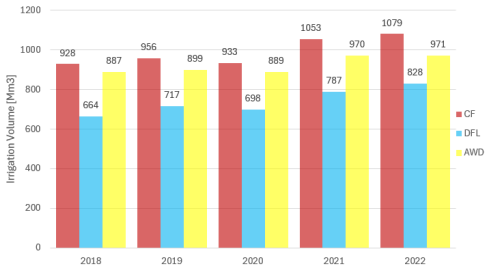

(b) DFL - mean

Figure 5.21: Statistic of Irrigation Volume and their evolution over time for the three different irrigation strategies over AIOS.

The irrigation volumes obtained for the AIOS district were computed by integrating the irrigation depths with the rice-cropped areas, as described in the methodology section. It is important to note that only for 2021 and 2022 the estimates are considered more reliable, since actual rice-cropped areas were available from the regional geoportal. For the previous years (2018–2020), such data were not accessible, and therefore the 2022 cropped area — representing an intermediate value between 2021 and 2023 — was used instead.

The resulting values show a clear interannual variability consistent with the trends observed for irrigation depth. During the first three years (2018–2020), irrigation volumes remain relatively stable for all three strategies, while from 2021 onward a significant increase is observed, reaching the maximum in 2022. The Continuous Flooding (CF) strategy records the highest average irrigation volume (987 Mm^3 over the five-year period), followed by Alternate Wetting and Drying (AWD) with 922 Mm^3, and Delayed Flooding (DFL) with 736 Mm^3, confirming its lower water demand.

5.5.6 Mean monthly Discharge

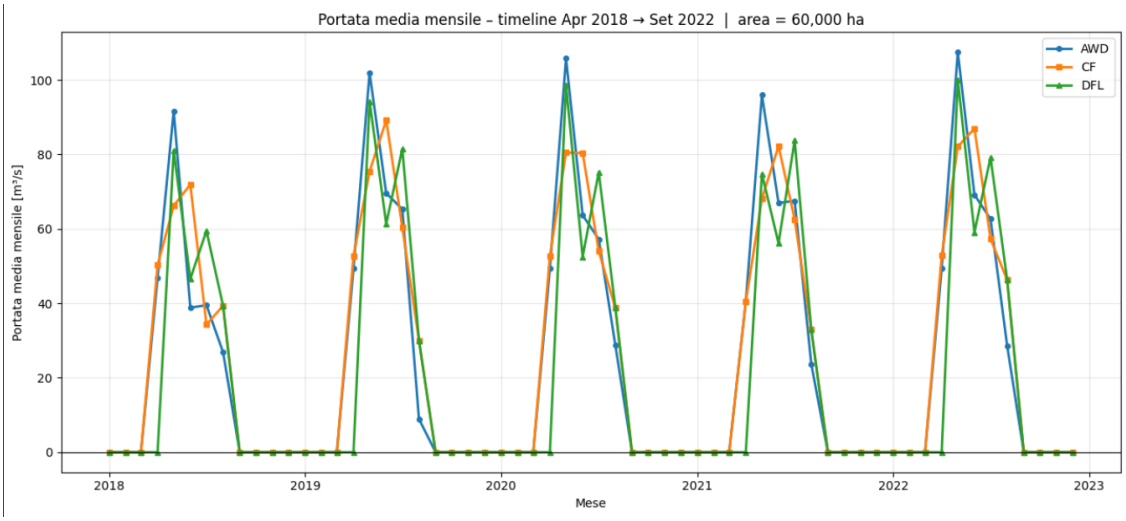

Figure 5.22: Mean monthly discharge

The mean monthly discharge trends over the 2018–2022 period highlight clear differences among the three irrigation strategies. Both CF and AWD show an early peak in discharge during the spring months, corresponding to the initial flooding phases. The results indicate that the peak values are comparable—or in some cases even higher—for AWD compared to CF. However, after this initial phase, AWD shows a rapid decline in discharge, with considerably lower values during the most critical summer months. This behavior represents a positive outcome, as it indicates a reduced water demand during periods of higher water lack.

The DFL strategy, on the other hand, presents overall lower discharge peaks that are shifted later in the season, with higher values occurring during the summer months. While this temporal delay contributes to a reduction in total water use, it can be problematic from a management perspective, since the highest discharges occur during the summer period when competition for water among different crops is at its maximum. Furthermore, the absence of early-season flooding limits the contribution to groundwater recharge that typically occurs during spring under CF and AWD, potentially reducing subsurface water availability later in the season.

5.6 Spatial Variation of Results

The spatial distribution of simulated irrigation requirements shows a clear dependence on climatic conditions across both the Po Basin and the AIOS sub-area. Scatter plots were used to assess the relationship between simulated irrigation requirements and both climatic (ET0, PRP) and pedological (FC) variables. For this purpose, seasonal aggregated values were used (cumulative ET0 and PRP, and total irrigation depth per pixel over the rice growing season) to capture the spatial variability across the study area. At both scales, a strong negative correlation between precipitation and irrigation depth and a positive correlation with reference evapotranspiration (ET0) are evident. Areas with higher rainfall correspond to lower irrigation requirements, while regions with greater evaporative demand show increased water needs. This consistent behaviour across all irrigation strategies (AWD, CF, and DFL) confirms that climate is the primary driver of irrigation demand variability, largely determining the spatial gradients observed in the simulated maps.

In contrast, the influence of soil properties is much weaker and appears to be scale-dependent. At the basin scale the scatter plots between irrigation depth and FC (Fig. 5.27a) reveal no evident correlation, and the data points are almost vertically aligned, indicating that irrigation depth is nearly insensitive to FC variations.

Within the AIOS sub-area, this weak soil influence becomes even less pronounced. The corresponding scatter plot (Fig. 5.29b) confirms the absence of a clear trend between FC and irrigation depth. Such consistency also depends on the fact that soil conditions are relatively homogeneous across the AIOS domain and therefore their influence is even less evident compared to the Po basin. Consequently it can be stated that climatic variability alone explains most of the spatial differences in irrigation demand.

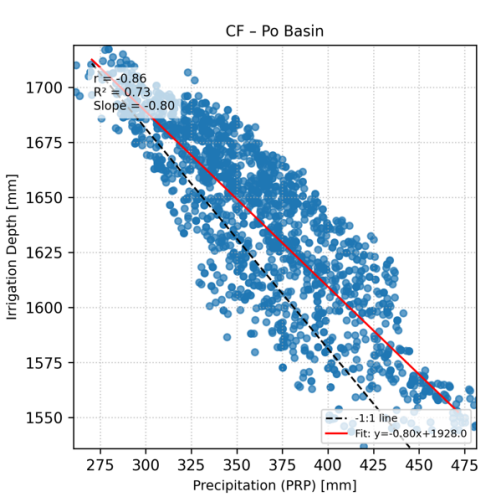

(a) PRP - Irr CF Po basin

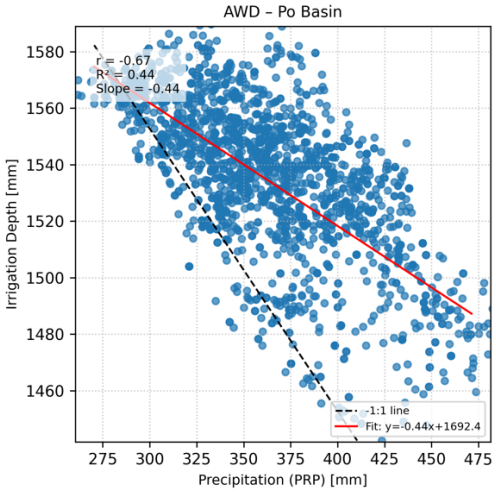

(b) PRP - Irr AWD Po basin

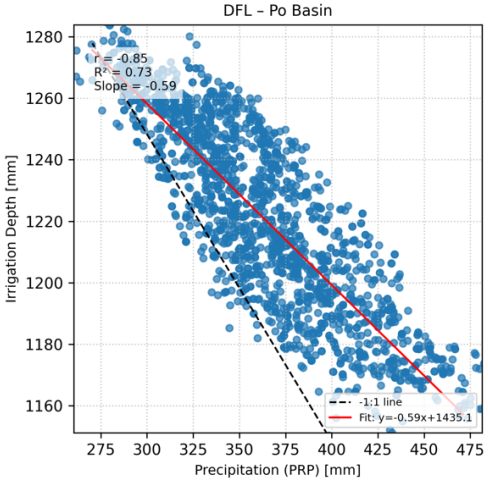

(c) PRP - Irr DFL Po basin

Figure 5.23: Correlation between simulated irrigation depth and precipitation (PRP) over the Po Basin. Both variables correspond to Rice growing season cumulative values derived from daily simulations. The strong negative correlation indicates that areas with higher rainfall experienced lower irrigation demand, highlighting the dominant climatic control on spatial irrigation variability

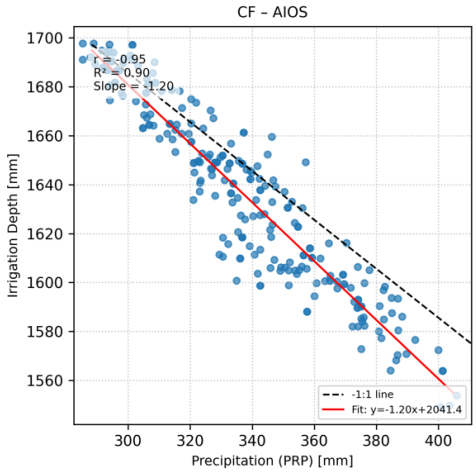

(a) PRP - Irr CF AIOS

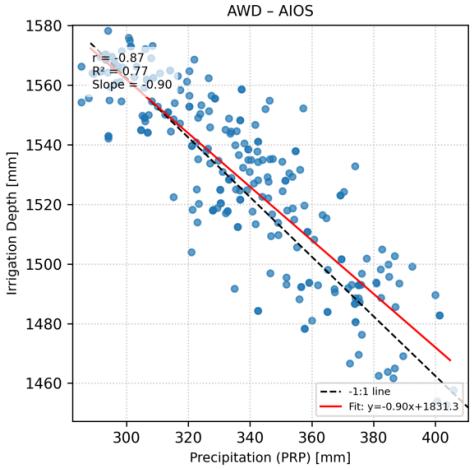

(b) PRP - Irr AWD AIOS

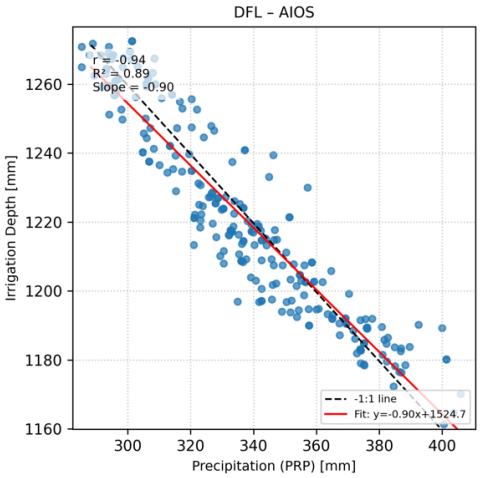

(c) PRP - Irr DFL AIOS

Figure 5.24: Correlation between simulated irrigation depth and precipitation (PRP) over AIOS. Both variables correspond to Rice growing season cumulative values derived from daily simulations. The strong negative correlation indicates that areas with higher rainfall experienced lower irrigation demand, highlighting the dominant climatic control on spatial irrigation variability

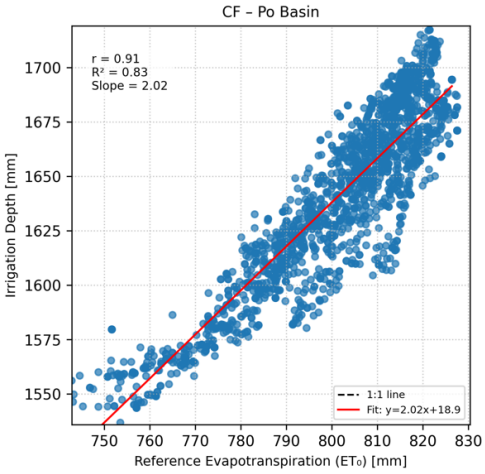

(a) ET0 - Irr CF Po basin

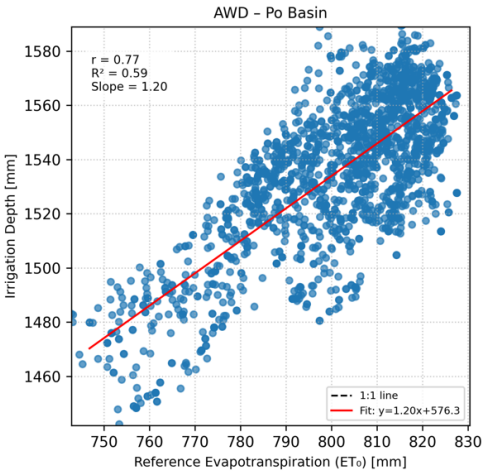

(b) ET0 - Irr AWD Po basin

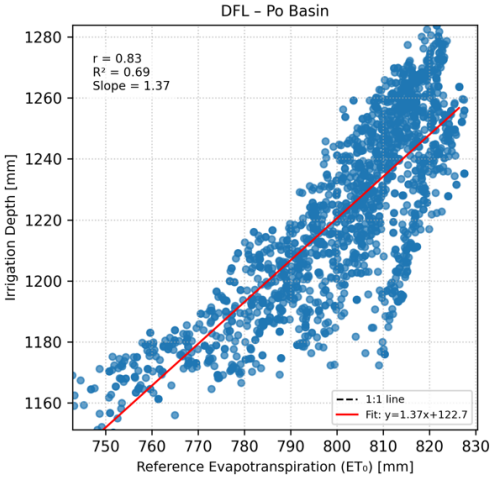

(c) ET0 - Irr DFL Po basin

Figure 5.25: Correlation between simulated irrigation depth and reference evapotranspiration (ET0) over the Po Basin for the three irrigation strategies (CF, AWD, and DFL). Both variables represent spatially aggregated seasonal totals (ET0 cumulative over the growing season and total simulated irrigation depth per pixel). The 1:1 line (dashed) and linear regression (red) illustrate the spatial relationship between climatic evaporative demand and irrigation requirements

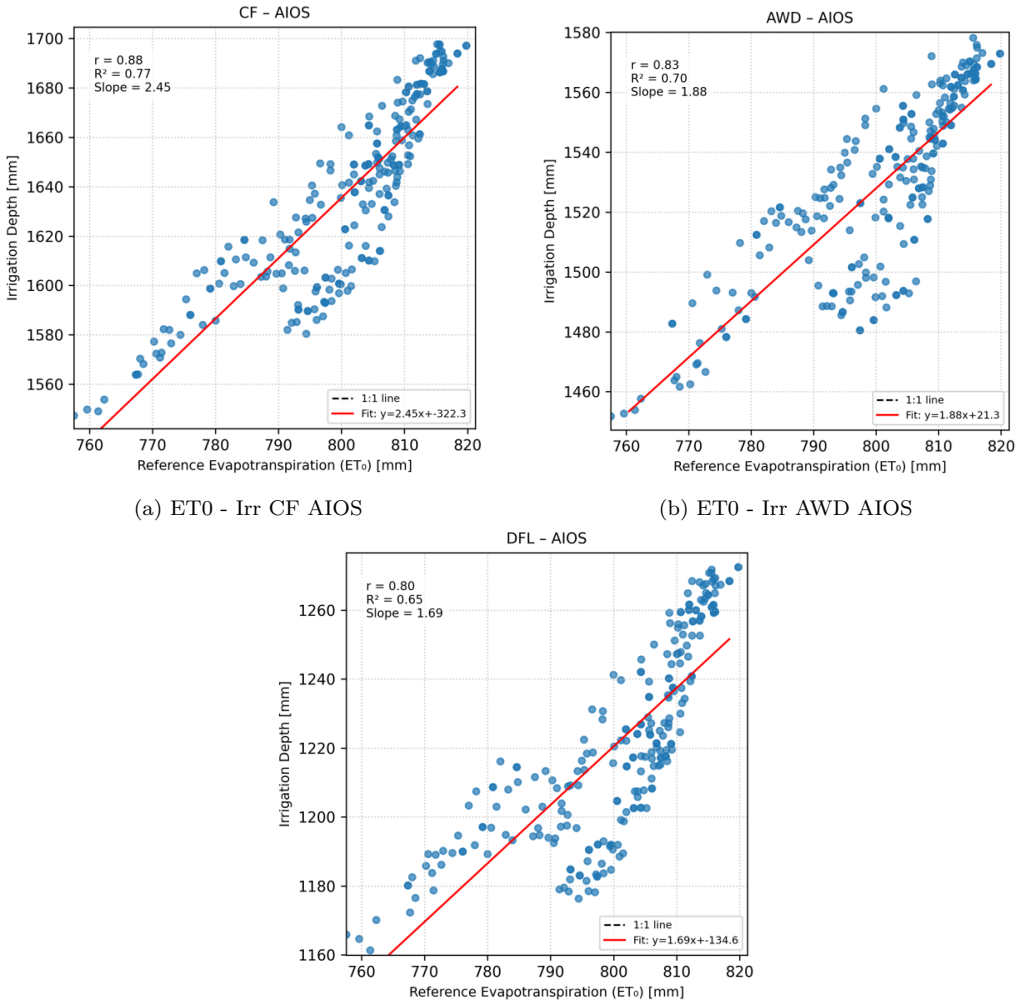

(a) ET0 - Irr CF AIOS

(b) ET0 - Irr AWD AIOS

(c) ET0 - Irr DFL AIOS

Figure 5.26: Correlation between simulated irrigation depth and reference evapotranspiration (ET0) over AIOS for the three irrigation strategies (CF, AWD, and DFL). Both variables represent spatially aggregated seasonal totals (ET0 cumulative over the growing season and total simulated irrigation depth per pixel). The 1:1 line (dashed) and linear regression (red) illustrate the spatial relationship between climatic evaporative demand and irrigation requirements

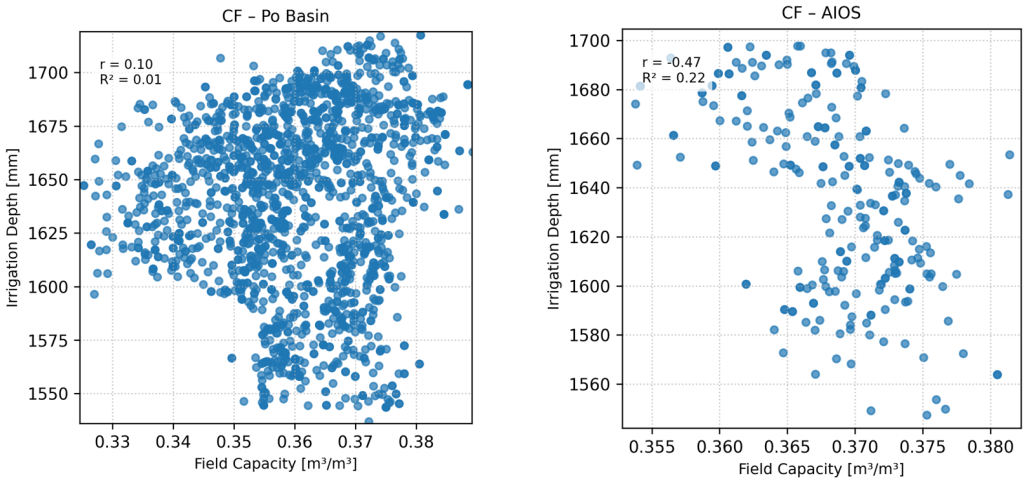

(a) IRR - FC Po Basin

(b) IRR - FC Po Basin AIOS

Figure 5.27: Scatter plots between field capacity (FC) and simulated irrigation depth over the Po Basin (a) and AIOS sub-area (b). FC values represent Soil Field Capacity, while irrigation depths are seasonal totals simulated under the CF management strategy. No clear correlation is observed, confirming the limited influence of soil texture on irrigation demand compared to climatic drivers.

Overall, these results highlight that the spatial variability of irrigation requirements is primarily driven by precipitation and evaporative demand, whereas pedological factors exert only a marginal control that becomes evident only at larger spatial scales—where greater heterogeneity in soil texture and hydraulic properties occurs.

Chapter 6

Conclusions

6.1 Summary and Critical discussion of Results

This thesis developed and applied a Python-based soil water balance model specifically designed for paddy rice cultivation in Northern Italy. The model, implemented on a daily time step and spatially integrated in a GIS framework, enabled the estimation of irrigation water requirements and the evaluation of three irrigation management strategies—Continuous Flooding (CF), Alternate Wetting and Drying (AWD), and Dry Seeding with Delayed Flooding (DFL)—across both the Po Basin and the AIOS irrigation district. The model showed a consistent hydrological behaviour and results coherent with literature, reproducing expected soil moisture and water level dynamics under different climatic and management conditions.

At both scales, irrigation requirements exhibited a clear sensitivity to interannual climatic variability. The driest year (2022) recorded the highest irrigation depths, while wetter years such as 2018 required substantially lower volumes. Among the tested strategies, CF resulted—as expected—in the largest water consumption, with average seasonal irrigation depths around 1650 mm. AWD reduced water use by approximately 7%, while DFL achieved the highest saving potential (around 25% less than CF). However, the DFL approach showed relevant drawbacks: by postponing the initial flooding phase, it concentrates irrigation demand during the critical summer months (June–August), when water availability is typically lowest and competition with other crops is highest. In contrast, AWD proved to be the most balanced and resilient strategy, combining moderate water savings with greater interannual stability. In fact when comparing the first and last years of the analysis (2018 vs. 2022), it can be observed that DFL shows the largest increase in irrigation depth, followed by CF, while AWD exhibits the smallest variation. This indicates that AWD is less sensitive to interannual climatic variability, making it a promising and more resilient irrigation strategy in the context of climate change adaptation. Moreover its alternating wetting and drying cycles allow substantial reduction in total irrigation demand while maintaining early-season flooding beneficial for groundwater recharge.

Beyond the temporal variability, the spatial analysis provided important insights into the drivers controlling irrigation demand. The spatial distribution of irrigation depth

across the Po Basin revealed strong and consistent correlations with climatic variables: a negative relationship with precipitation and a positive relationship with reference evapotranspiration (ET0), confirming that climate is the dominant control on irrigation variability. The same trend was observed within the AIOS sub-area, indicating that local-scale patterns are mainly governed by rainfall and evaporative demand rather than by soil heterogeneity.

In contrast, the influence of soil properties appeared scale-dependent and overall weaker. At the basin scale, the relationship between field capacity (FC) and sand content (Fig. 5.7 and 5.8) revealed a distinct textural gradient, with finer soils showing higher FC values. However, scatter plots between irrigation depth and FC (Fig. 5.29a) did not display any meaningful correlation. The slight positive trend observed—indicating higher irrigation demand with increasing FC—is physically inconsistent, since soils with greater water-holding capacity should, in principle, require less irrigation. This inversion highlights that spatial variability in irrigation depth is mainly driven by climatic forcing rather than by soil hydraulic properties. Within the AIOS area, this pattern is even more evident: the maps of FC and sand content (Fig. 5.9) and their scatter relationship (Fig. 5.10) show a nearly absent correlation, reflecting the homogeneous soil texture across the district. Consequently, the weak or reversed relationships observed between irrigation depth and FC represent indirect evidence that climatic gradients (precipitation and ET0) largely control irrigation demand, whereas pedological factors play only a marginal role.

Beyond the numerical results, the study highlights the importance of modelling approaches for supporting sustainable water management in rice- growing districts. By integrating climatic, soil, and crop data at high spatial resolution, the developed model provides a valuable tool for irrigation authorities and decision-makers to identify water-saving opportunities, evaluate management alternatives, and plan more efficient allocation strategies. Overall, this work contributes to improving the under-standing of irrigation dynamics in Mediterranean rice systems and offers a reproducible methodological framework for future applications aimed at enhancing agricultural water efficiency and resilience to climate change.

6.2 Limitations and future works

The model developed in this study presents some limitations that should be addressed in future improvements. First, deep percolation (DP) is currently considered as a constant daily value across the entire study area, without accounting for spatial variability related to different soil properties. Future developments should aim to introduce spatial heterogeneity, either by applying pedotransfer equations or by conducting field measurement campaigns to better characterize soil hydraulic properties and infiltration behavior. Moreover, groundwater level (GWL) dynamics are not included in the current model. In reality, the groundwater table is typically recharged during the initial flooding phases under CF and AWD strategies and becomes very shallow during the summer months, providing additional water that helps reduce irrigation demand—especially in downstream areas. Including this process would likely result in lower irrigation requirements for CF

and AWD, or at least a relative increase for DFL due to its delayed flooding period. Another important limitation is that the model operates under theoretical conditions of unlimited water availability. It assumes that the irrigation water required by the crop is always fully supplied, without considering possible water shortages or allocation limits. Incorporating real discharge data and measured irrigation volumes would allow for a more realistic simulation of water distribution and potential supply constraints. Additionally, the lack of detailed data regarding the actual distribution of irrigation strategies within the AIOS area prevents the estimation of real irrigation volumes at the district scale. Having these percentages would enable more accurate irrigation requirements assessments for the district. By addressing these aspects, the model could evolve into a powerful tool not only for estimating irrigation volumes but also for real-time monitoring and decision support. Continuous field measurements are often difficult and costly to obtain; therefore, a model capable of simulating the daily hydrological status of rice fields could become an effective management support system. In future developments, the integration of short-term weather forecasts could further enhance its predictive capability, enabling the forecast of soil moisture conditions and the implementation of more efficient irrigation scheduling strategies.

List of Figures

List of Tables

Bibliography

[1] GCEW. The what, why and how of the world water crisis: Global commission on the economics of water phase 1 review and findings,, 2023. URL https://watercommission.org/publication/phase-1-review-and-findings/.

[2] World Meteorological Organization (WMO). 2021 state of climate services, 2021. URL https://library.wmo.int/records/item/57630-2021-state-of-climate-services-water?offset=2.

[3] Petra Doell and Stefan Siebert. Global modeling of irrigation water requirements. *Water Resources Research*, 38:8–1, 04 2002. doi: 10.1029/2001wr000355.

[4] FAO. Water for sustainable food and agriculture, 2016. URL https://openknowledge.fao.org/items/41d13416-d012-47b2-9ea6-5731949b65c5.

[5] Qiu Haonan, Wang Jie, Shihong Yang, Zewei Jiang, and Xu Yi. Current status of global rice water use efficiency and water-saving irrigation technology recommendations. *Journal of Agronomy and Crop Science*, 209, 05 2023. doi: 10.1111/jac.12655.

[6] Orasen Gabriele, Patrizia Nisi, Giorgio Lucchini, Alessandro Abruzzese, Michele Pesenti, Moez Maghrebi, Ajay Kumar, Fabio Nocito, Elena Baldoni, Silvia Morgutti, Noemi Negrini, Giampiero Valè, and Gian Sacchi. Continuous flooding or alternate wetting and drying differently affect the accumulation of health-promoting phytochemicals and minerals in rice brown grain. *Agronomy*, 9, 10 2019. doi: 10.3390/agronomy9100628.

[7] R. Wassmann, Krishna Jagadish, Sigrid Heuer, A.M. Ismail, E. Redona, Rachid Serraj, Rakesh Singh, G. Howell, Dr Surendra Pathak, and K. Sumfleth. Climate change affecting rice production: The physiological and agronomic basis for possible adaptation strategies. *Advances in Agronomy*, 101, 01 2009.

[8] Bas Bouman, E. Humphreys, T.P. Tuong, and Randolph Barker. Rice and water. *Advances in Agronomy*, 92:187–237, 12 2007. doi: 10.1016/S0065-2113(04)92004-4.

[9] Alice Mayer, Michele Rienzner, Sandra Cesari de Maria, Marco Romani, Alberto Lasagna, and Arianna Facchi. A comprehensive modelling approach to assess water use efficiencies of different irrigation management options in rice irrigation districts of northern italy. *Water*, 11(9), 2019. ISSN 2073-4441. doi: 10.3390/w11091833. URL https://www.mdpi.com/2073-4441/11/9/1833.

[10] Matteo Rolle, Stefania Tamea, and Pierluigi Claps. Era5-based global assessment of irrigation requirement and validation. *PLOS ONE*, 16:e0250979, 04 2021. doi: 10.1371/journal.pone.0250979.

[11] Richard Allen, L. Pereira, Dirk Raes, and M. Smith. Fao irrigation and drainage paper no. 56. *Rome: Food and Agriculture Organization of the United Nations*, 56: 26–40, 01 1998.

[12] U.S. Army Corps of Engineers, Hydrologic Engineering Center. *HEC-HMS Technical Reference Manual*. USACE, Davis, California, 2025. URL `https://www.hec.usace.army.mil/confluence/hmsdocs/hmstrm`. Version 4.13.

[13] Suhua Liu, Hongbo Su, Renhua Zhang, Jing Tian, Shaohui Chen, and Wang Weizhen. Regional estimation of remotely sensed evapotranspiration using the surface energy balance-advection (seb-a) method. *Remote Sensing*, 8:644, 08 2016. doi: 10.3390/rs8080644.

[14] Petra Doell and Stefan Siebert. Global modeling of irrigation water requirements. *Water Resources Research*, 38:8–1, 04 2002. doi: 10.1029/2001wr000355.

[15] Charlotte Fraiture. Integrated water and food analysis at the global and basin level. an application of watersim. *Water Resources Management*, 21:185–198, 09 2007. doi: 10.1007/s11269-006-9048-9.

[16] Stefanie Rost, Dieter Gerten, Alberte Bondeau, Wolfgang Lucht, Janine Rohwer, and Sibyll Schaphoff. Agricultural green and blue water consumption and its influence on the global water system. *Water Resour. Res*, 44, 09 2008. doi: 10.1029/2007WR006331.

[17] Naota Hanasaki, Sawase Kanae, Taikan Oki, Masuda K, Kiyoichiro Motoya, Shirakawa N, Yanjun Shen, and Kenji Tanaka. An integrated model for the assessment of global water resources part 1: Model description and input meteorological forcing. *Hydrology and Earth System Sciences*, 12, 07 2008. doi: 10.5194/hess-12-1007-2008.

[18] Stefan Siebert and Petra Doell. Quantifying blue and green virtual water contents in global crop production as well as potential production losses without irrigation. *Journal of Hydrology*, 384:198–217, 04 2010. doi: 10.1016/j.jhydrol.2009.07.031.

[19] Junguo Liu and Hong Yang. Spatially explicit assessment of global consumptive water uses in cropland: Green and blue water. *Journal of Hydrology*, 384:187–197, 11 2009. doi: 10.1016/j.jhydrol.2009.11.024.

[20] Mesfin Mekonnen and Arjen Hoekstra. The green, blue and grey water footprint of crops and derived crop products. *Hydrology and Earth System Sciences Discussions*, 8, 01 2011. doi: 10.5194/hessd-8-763-2011.

[21] Rosa et al Chiarelli, Passera. The green and blue crop water requirement watneeds model and its global gridded outputs. *Scientific Data 7*, 7, 08 2020. doi: 10.1038/s41597-020-00612-0.

[22] Rina Vuciterna, Giordano Ruggeri, Stefano Corsi, Arianna Facchi, and Olfa Gharsallah. A bibliometric analysis of scientific literature on alternate wetting and drying (awd). *Paddy and Water Environment*, 22, 05 2024. doi: 10.1007/s10333-024-00975-9.

[23] Giulio Gilardi, Alice Mayer, Michele Rienzner, Marco Romani, and Arianna Facchi. Effect of alternate wetting and drying (awd) and other irrigation management strategies on water resources in rice-producing areas of northern italy. *Water*, 15: 2150, 06 2023. doi: 10.3390/w15122150.

[24] Food and Agriculture Organization of the United Nations (FAO) and International Rice Research Institute (IRRI). Rice farming: saving water through alternate wetting and drying (awd) method, indonesia. TECA - Technologies and Practices for Small Agricultural Producers, 2013. URL `https://www.fao.org/teca/en/practice/rice-farming-saving-water-through-alternate-wetting-and-drying-awd-method-indonesia`. Practice ID: 7939.

[25] Arianna Facchi, Dmytro Tkachenko, Matteo Rienzner, Giulia Gilardi, Paolo Mascherpa, and Bruno Ortuani. Progetto risosost: Percorsi agronomici innovativi per una risicoltura sostenibile. monitoraggio degli aspetti idrologici relativi alla tecnica awd e alla sommersione invernale. Presentation, DiSAA – Università degli Studi di Milano, 2024. Finanziato nell'ambito del Programma di Sviluppo Rurale 2014–2022, Operazione 16.2.01.

[26] Daniela R. Carrijo, Mark E. Lundy, and Bruce A. Linquist. Rice yields and water use under alternate wetting and drying irrigation: A meta-analysis. *Field Crops Research*, 203:173–180, 2017. ISSN 0378-4290. doi: https://doi.org/10.1016/j.fcr.2016.12.002. URL `https://www.sciencedirect.com/science/article/pii/S0378429016307791`.

[27] Arianna Facchi and Legambiente Lombardia. La riduzione delle emissioni di metano in risicoltura. Technical report, Legambiente Lombardia, 2025. Presentazione: *Factsheet_Riso e clima_Legambiente_Lombardia*.

[28] Eleonora Miniotti, Marco Romani, Daniel Said-Pullicino, Arianna Facchi, Chiara Bertora, Matteo Peyron, Dario Sacco, Gian Battista Bischetti, Cristina Lerda, Daniele Tenni, Claudio Gandolfi, and Luisella Celi. Agro-environmental sustainability of different water management practices in temperate rice agro-ecosystems. *Agriculture, Ecosystems Environment*, 222:235–248, 04 2016. doi: 10.1016/j.agee.2016.02.010.

[29] Lucia Crosetto. Adozione della sommersione invernale e awd per la mitigazione delle emissioni di metano. Conference presentation, Università degli Studi di Torino, Dipartimento di Scienze Agrarie, Forestali e Alimentari (DISAFA), 2024.

[30] ANBI. Associazione nazionale bonifiche, irrigazioni e miglioramenti fondiari (anbi)-accessible at https://www.anbi.it/p/chi-siamo.

[31] Associazione Nazionale Bonifiche, Irrigazioni e Miglioramenti Fondiari (ANBI). Nota informativa anbi - consorzi di bonifica e piano laghetti. Institutional report, 2025. URL https://www.anbi.it/p/chi-siamo. Accessed: October 29, 2025.

[32] ANBI PIEMONTE. Anbi piemonte accessible at, . URL https://anbipiemonte.it.

[33] Associazione D'Irrigazione Ovest Sesia AIOS. Associazione d'irrigazione ovest sesia -aios accessible at. URL https://www.ovestsesia.it.

[34] SIBI. Sibi accessible at. URL https://www.regione.piemonte.it/web/temi/agricoltura/agroambiente-meteo-suoli/bonifica-irrigazione-sibi.

[35] GEOPORTALE PIEMONTE. Geoportale piemonte accessible at, . URL https://geoportale.igr.piemonte.it/cms/.

[36] ARPA Piemonte. Il clima in piemonte nel 2022, January 2023. URL https://www.arpa.piemonte.it/. Dipartimento Rischi Naturali e Ambientali. Report tecnico annuale.

[37] Mario Raffa, Alfredo Reder, Gian Franco Marras, Marco Mancini, Gabriella Scipione, Monia Santini, and Paola Mercogliano. Vhr-rea-it dataset: Very high resolution dynamical downscaling of era5 reanalysis over italy by cosmo-clm. *Data*, 6(8), 2021. ISSN 2306-5729. doi: 10.3390/data6080088. URL https://www.mdpi.com/2306-5729/6/8/88.

[38] Mario Raffa, Alfredo Reder, and Paola Mercogliano. D4.1 datasets of downscaled era5 reanalysis over italy, 2021. URL https://highlanderproject.eu/. Highlander Project, Co-financed by the Connecting Europe Facility of the European Union.

[39] SOILGRIDS. Soilgrids documentation accessible at. URL https://docs.isric.org/globaldata/soilgrids/.

[40] T. de Boer-Euser, L. Bouaziz, H. Winsemius, A. de Roo, and H. H. G. Savenije. Hihydrosoil v2.0: High resolution soil maps of global hydraulic properties. Technical report, FutureWater, Wageningen, The Netherlands, 2020. URL https://www.futurewater.nl/wp-content/uploads/2020/10/HiHydroSoil-v2.0-High-Resolution-Soil-Maps-of-Global-Hydraulic-Properties_v2.pdf. Technical Report, October 2020.

[41] Pierluigi Claps, Francesco Laio, and Luca Grossini. Valutazione dei consumi e dei fabbisogni idrici nel comprensorio irriguo denominato centro sesia su una superficie di circa 15.500 ettari. Technical report, Politecnico di Torino, Dipartimento di Idraulica, Trasporti ed Infrastrutture Civili (DITIC), Torino, Italia, 2008. Report tecnico per il Consorzio di Bonifica della Baraggia Biellese e Vercellese.

[42] ENR - ENTE NAZIONALE RISO. Linee guida per l'implementazione della tecnica irrigua alternate wetting and drying (awd) associata alla semina in acqua del riso, 2024. linee guida operative AWD - RISWAGEST Project.

[43] Manuel Campos-Taberner, Francisco Javier García-Haro, Lorenzo Busetto, Luigi Ranghetti, Beatriz Martínez, María Amparo Gilabert, Gustau Camps-Valls, Fernando Camacho, and Mirco Boschetti. A critical comparison of remote sensing leaf area index estimates over rice-cultivated areas: From sentinel-2 and landsat-7/8 to modis, geov1 and eumetsat polar system. *Remote Sensing*, 10(5), 2018. ISSN 2072-4292. doi: 10.3390/rs10050763. URL https://www.mdpi.com/2072-4292/10/5/763.

[44] Giacomo Fontanelli, Daniela Stroppiana, Ramin Azar, Lorenzo Busetto, Mirco Boschetti, Luca Gatti, F. Collivignarelli, M. Barbieri, and F. Holecz. Rice monitoring using sar and optical data in northern italy, 07 2015.

[45] Numpy. Numpy documentation accessible at. URL https://numpy.org/doc/stable/user/absolute_beginners.html.

[46] Pandas. Pandas documentation accessible at. URL https://pandas.pydata.org/docs/getting_started/index.html.

[47] Xarray. Xarray documentation accessible at. URL https://docs.xarray.dev/en/stable/getting-started-guide/why-xarray.html.

[48] Qgis. Qgis introduction. URL https://docs.qgis.org/3.28/pdf/en/QGIS-3.28-GentleGISIntroduction-en.pdf.